Author Manuscript

Author Manuscript

Author Manuscript

Author Manuscript

HHS Public Access

Author manuscript

Science. Author manuscript; available in PMC 2021 June 16.

Published in final edited form as:

Science. 2021 March 05; 371(6533): . doi:10.1126/science.abc8697.

Targeting a neoantigen derived from a common *TP53* mutation

Emily Han-Chung Hsiue[#1,2,3], **Katharine M. Wright**[#2,4,5], **Jacqueline Douglass**[#1,2,3], **Michael S. Hwang**[1,2,3], **Brian J. Mog**[1,2,3,6], **Alexander H. Pearlman**[1,2,3], **Suman Paul**[1,2,3,7], **Sarah R. DiNapoli**[1,2,3], **Maximilian F. Konig**[1,2,3,8], **Qing Wang**[1,2,9], **Annika Schaefer**[1,2,3], **Michelle S. Miller**[2,4,5,†], **Andrew D. Skora**[1,2,‡], **P. Aitana Azurmendi**[2,4,5], **Michael B. Murphy**[10], **Qiang Liu**[1,2,3], **Evangeline Watson**[1,2,3], **Yana Li**[4], **Drew M. Pardoll**[5,7], **Chetan Bettegowda**[1,3,11], **Nickolas Papadopoulos**[1,3,5,12], **Kenneth W. Kinzler**[1,3,5], **Bert Vogelstein**[1,2,3,5,12,§], **Sandra B. Gabelli**[4,7,13,§], **Shibin Zhou**[1,3,5,§]

[1]Ludwig Center, Sidney Kimmel Comprehensive Cancer Center, Johns Hopkins University School of Medicine, Baltimore, MD 21287, USA.

[2]Howard Hughes Medical Institute, Chevy Chase, MD 20815, USA.

PERMISSIONS http://www.sciencemag.org/help/reprints-and-permissions

[§]Corresponding author. vogelbe@jhmi.edu (B.V.); gabelli@jhmi.edu (S.B.G.); sbzhou@jhmi.edu (S.Z.).
[†]Present address: Walter and Eliza Hall Institute of Medical Research and Department of Medical Biology, University of Melbourne, VIC 3052, Australia.
[‡]Present address: Lilly Biotechnology Center, Eli Lilly and Co, San Diego, CA 92121, USA.

Author contributions: Conceptualization: E.H.H., K.M.W., J.D., M.S.H., B.J.M., A.H.P., A.D.S., N.P., K.W.K., B.V., S.B,G., and S.Z.; Methodology: E.H.H., K.M.W., J.D., Q.W., M.S.H., B.J.M., A.H.P., A.D.S., and M.S.M.; Investigation: E.H.H., K.M.W., Q.W., A.S., S.R.D., P.A.A., M.B.M., Q.L., E.W., and Y.L.; Analysis and interpretation of data: E.H.H., K.M.W., J.D., Q.W., M.S.H., B.J.M., A.H.P., S.P., S.R.D., M.F.K., D.M.P., C.B., N.P., K.W.K., S.B.G., B.V., and S.Z.; Writing–original draft: E.H.H. and K.M.W.; Writing–review and editing: D.M.P., C.B., N.P., K.W.K., S.B.G., B.V., and S.Z.; Supervision: C.B., N.P., K.W.K., S.B.G., B.V., and S.Z.

Competing interests: The Johns Hopkins University has filed patent applications related to technologies described in this paper on which E.H.H., K.M.W., J.D., Q.W., M.S.H., B.J.M., A.H.P., A.D.S., N.P., K.W.K., B.V., S.B.G., and S.Z. are listed as inventors: HLA-restricted epitopes encoded by somatically mutated genes (US20180086832A1), MANAbodies and methods of using (US20200079854A1), MANAbodies targeting tumor antigens and methods of using (PCT/US2020/065617). B.V., K.W.K., and N.P. are founders of Thrive Earlier Detection. K.W.K. and N.P. are consultants to and were on the Board of Directors of Thrive Earlier Detection. B.V., K.W.K., N.P., and S.Z. own equity in Exact Sciences. B.V., K.W.K., N.P., S.Z., and D.M.P. are founders of, hold or may hold equity in, and serve or may serve as consultants to ManaT Bio. B.V., K.W.K., N.P., and S.Z. are founders of, hold equity in, and serve as consultants to Personal Genome Diagnostics. S.Z. has a research agreement with BioMed Valley Discoveries. S.B.G. is a founder and holds equity in AMS. K.W.K. and B.V. are consultants to Sysmex, Eisai, and CAGE Pharma and hold equity in CAGE Pharma. B.V. is also a consultant to Catalio. K.W.K., B.V., S.Z., and N.P. are consultants to and hold equity in NeoPhore. N.P. is an advisor to and holds equity in CAGE Pharma. C.B. is a consultant to Depuy-Synthes and Bionaut Pharmaceuticals. The companies named above, as well as other companies, have licensed previously described technologies related to this paper from Johns Hopkins University. B.V., K.W.K., S.Z., N.P., and C.B. are inventors on some of these technologies. Licenses to these technologies are or will be associated with equity or royalty payments to the inventors as well as to Johns Hopkins University. The terms of all these arrangements are being managed by Johns Hopkins University in accordance with its conflict of interest policies. Q.W. is the founder and CEO of Complete Omics. M.F.K. received personal fees from Bristol-Myers Squibb and Celltrion. D.M.P. reports grant and patent royalties through institution from BMS, a grant from Compugen, stock from Trieza Therapeutics and Dracen Pharmaceuticals, and founder equity from Potenza; being a consultant for Aduro Biotech, Amgen, Astra Zeneca (Medimmune/Amplimmune), Bayer, DNAtrix, Dynavax Technologies Corporation, Ervaxx, FLX Bio, Rock Springs Capital, Janssen, Merck, Tizona, and Immunomic-Therapeutics; being on the scientific advisory board of Five Prime Therapeutics, Camden Nexus II, WindMil; and being on the board of directors for Dracen Pharmaceuticals.

Data and materials availability:
The MS data have been deposited with ProteomeXchange and can be accessed through identifier PASS01521. The H2-Fab–$p53^{R175H}$/HLA-A*02:01 ternary complex has been deposited in the Worldwide PDB with accession code 6W51. All materials will be made available to the scientific community through a materials transfer agreement from Johns Hopkins University.

SUPPLEMENTARY MATERIALS
science.sciencemag.org/content/371/6533/eabc8697/suppl/DC1

Author Manuscript Author Manuscript Author Manuscript Author Manuscript

[3]Lustgarten Pancreatic Cancer Research Laboratory, Sidney Kimmel Comprehensive Cancer Center, Johns Hopkins University School of Medicine, Baltimore, MD 21287, USA.

[4]Department of Biophysics and Biophysical Chemistry, Johns Hopkins University School of Medicine, Baltimore, MD 21287, USA.

[5]Bloomberg~Kimmel Institute for Cancer Immunotherapy, Sidney Kimmel Comprehensive Cancer Center, Baltimore, MD 21287, USA.

[6]Department of Biomedical Engineering, Johns Hopkins University, Baltimore, MD 21218, USA.

[7]Department of Oncology, Johns Hopkins University School of Medicine, Baltimore, MD 21287, USA.

[8]Division of Rheumatology, Department of Medicine, Johns Hopkins University School of Medicine, Baltimore, MD 21224, USA.

[9]Complete Omics, Baltimore, MD 21227, USA.

[10]Cytiva, Marlborough, MA 01752, USA.

[11]Department of Neurosurgery, Johns Hopkins University School of Medicine, MD 21205, USA.

[12]Department of Pathology, Johns Hopkins University School of Medicine, Baltimore, MD 21205, USA.

[13]Department of Medicine, Johns Hopkins University School of Medicine, Baltimore, MD 21205, USA.

[#] These authors contributed equally to this work.

Abstract

TP53 (tumor protein p53) is the most commonly mutated cancer driver gene, but drugs that target mutant tumor suppressor genes, such as *TP53*, are not yet available. Here, we describe the identification of an antibody highly specific to the most common *TP53* mutation (R175H, in which arginine at position 175 is replaced with histidine) in complex with a common human leukocyte antigen–A (HLA-A) allele on the cell surface. We describe the structural basis of this specificity and its conversion into an immunotherapeutic agent: a bispecific single-chain diabody. Despite the extremely low p53 peptide-HLA complex density on the cancer cell surface, the bispecific antibody effectively activated T cells to lyse cancer cells that presented the neoantigen in vitro and in mice. This approach could in theory be used to target cancers containing mutations that are difficult to target in conventional ways.

Targeted therapies, such as trastuzumab and imatinib, have revolutionized the treatment of cancer patients. All such drugs used thus far in the clinic target oncogenes rather than tumor suppressor genes. This is because drugs generally inhibit the action of proteins, and oncogenic proteins are activated by mutations or amplifications. By contrast, the proteins encoded by tumor suppressor genes are already inactivated, and reactivation is extremely difficult or impossible, depending on the nature of the alteration. This challenge is highlighted by *TP53* (tumor protein p53), which was the first tumor suppressor gene identified and is inactivated in the great majority of human tumors (1-4). Despite extensive

Author Manuscript Author Manuscript Author Manuscript Author Manuscript

efforts, no drug that targets mutant p53 has been approved for treatment of the large number of patients whose tumors contain these mutations.

Mutations in *TP53* most commonly occur as single-nucleotide variants at positions that cluster in the DNA-binding domain (5, 6). Proteins derived from mutant *TP53* alleles can be degraded by the proteasome, processed, and presented by the major histocompatibility complex to generate neoantigens recognizable by T cell receptors (TCRs) (7, 8). R175H, in which arginine at position 175 is replaced with histidine, is the most common mutation observed in *TP53* as well as the most frequent mutation in any tumor suppressor gene (9). The peptide HMTEVVRHC (mutant amino acid underlined), derived from $p53^{R175H}$, binds to a human leukocyte antigen (HLA) allele (A*02:01) that is present in more than 40% of U.S. Caucasians (8, 10).

Peptide-HLA (pHLA) complexes are the natural ligands for TCRs. Recently, TCR-mimic (TCRm) antibodies have emerged as a class of agents that target pHLA derived from intracellular proteins in cancer cells (11-14). Compared with TCRs, TCRm antibodies are of higher affinity and can be easily converted to various therapeutic formats such as full-length antibodies, antibody-drug conjugates, and bispecific antibodies (11-15). TCRs as well as TCRm antibodies can also be used for T cell–based therapies, such as those using engineered TCRs or chimeric antigen receptors, respectively (16, 17). Such cell-based therapies have been remarkably successful for the treatment of certain cancers (18-21) but require individualized development of autologous cells from each patient (22). On the other hand, T cell–retargeting bispecific antibodies, with dual specificities for a tumor antigen and for the TCR-CD3 complex, are off-the-shelf reagents that can theoretically be used to treat any patient whose tumors contain the targeted antigen. One end of the bispecific antibody binds to the tumor cell, and the other end triggers T cell cytotoxicity and cytokine production in a tumor-selective fashion. This format has mainly been developed to target highly expressed, non–tumor-specific, wild-type (WT) cell surface proteins (23). One example is blinatumomab, a potent bispecific antibody that targets the pan–B cell antigen CD19 and has been approved for the treatment of B cell leukemias (24).

Here, we describe the identification of a TCRm antibody specific to the HLA-A*02:01-restricted $p53^{R175H}$ neoantigen, the structural basis of its specificity, and its conversion to a bispecific antibody that can lyse cancer cells in a fashion dependent on the presence of the neoantigen.

Results

The $p53^{R175H}$ neoantigen is presented on the surface of cancer cells

The $p53^{R175H}$ (amino acids 168 to 176, HMTEVVRHC) and $p53^{WT}$ (HMTEVVRRC) peptides were predicted on the NetMHCpan 4.0 server to bind HLA-A*02:01 at 5177.6 nM (rank 9.7%) and 7121.5 nM (11.6%), respectively (25). Although such predictions are useful for prioritization, they are not a reliable way to determine whether a potential neoantigen is actually presented on the cell surface (26). To provide experimental evidence of and to quantify such presentation, we analyzed peptides eluted from HLA molecules in four different cell culture systems using a mass spectrometry (MS)–based method (27). First, the

Author Manuscript Author Manuscript Author Manuscript Author Manuscript

human HLA-A*02:01 and either full-length $p53^{R175H}$ or $p53^{WT}$ were coexpressed in monkey COS-7 cells. MS analysis of the peptides that were immunopurified with an antibody to HLA detected the $p53^{R175H}$ peptide at approximately 700 copies per cell (fig. S1A and table S1). Although we detected relatively abundant amounts of the $p53^{R175H}$ peptide, we did not observe the $p53^{WT}$ peptide in pHLA complexes in transfected cells, despite equivalent amounts of $p53^{WT}$ and $p53^{R175H}$ total protein expression, as assessed with Western blotting (fig. S1B). Second, we performed MS analysis on three human cancer cell lines—KMS26, TYK-nu, and KLE—all of which harbor the $p53^{R175H}$ mutation and carry an HLA-A*02:01 allele (8). The $p53^{R175H}$ peptide was detected on all three cell lines and, as expected, at much lower levels than in the COS-7 cells in which the mutant *TP53* and HLA genes were exogenously introduced (fig. S1C and table S1). On the basis of comparisons with heavy isotope–labeled controls, we estimated that there were 2.4, 1.3, and 1.5 copies of $p53^{R175H}$/HLA-A*02:01 complexes on the cell surfaces of KMS26, KLE, and TYK-nu cell lines, respectively (table S1).

Identification of scFv-expressing phage clones specific for the HLA-A*02:01–restricted $p53^{R175H}$ peptide and conversion to scDb format

To identify TCRm single-chain variable fragments (scFvs) that selectively target mutant pHLA complexes, we screened an scFv-displaying phage library with an estimated complexity of $>1 \times 10^{10}$ (28). Positive selection against HLA-A*02:01 pHLA monomers that contain the $p53^{R175H}$ peptide was combined with negative selection against pHLA monomers that contain the $p53^{WT}$ and irrelevant peptides. Selected phage clones were amplified and assessed by means of flow cytometry for binding to T2 cells that present the mutant or WT peptide (fig. S2A).

Twenty-three phage clones with median fluorescence intensity (MFI) ratios of $p53^{R175H}$ to $p53^{WT}$ >4 were then converted to T cell–retargeting bispecific antibodies. This was achieved through linking each individual scFv to an anti-$CD3_\varepsilon$ scFv (UCHT1) in a single-chain diabody (scDb) format (fig. S2B). The scDb format was chosen after evaluating several bispecific antibody formats—such as bispecific T cell engagers (BiTE), dual-affinity retargeting antibodies (DARTs), and diabodies—in experiments assessing other antigens (29, 30). The ability of scDbs to activate T cells was assessed from interferon-γ (IFN-γ) release alter co-incubation with COS-7 cells overexpressing HLA-A*02:01 and either full-length $p53^{WT}$ or $p53^{R175H}$ proteins. Two scDb clones—named H2-scDb and H20-scDb and derived from phage clones H2 and H20, respectively—showed the most potent and specific T cell activation in the presence of $p53^{R175H}$/HLA-A*02:01 (fig. S2C and table S2). The specificity of these scDbs was further evaluated with titration enzyme-linked immunosorbent assay (ELISA). Both H2- and H20-scDbs bound to $p53^{R175H}$/HLA-A*02:01 at low concentrations, as expected. At high concentrations, H20-scDb also bound to $p53^{WT}$/HLA-A*02:01, whereas H2-scDb did not bind to the WT pHLA complex even at very high concentrations of the scDb (Fig. 1A and fig. S2D). H2-scDb was therefore chosen for further analysis. As assessed with surface plasmon resonance (SPR), the H2-scDb bound to $p53^{R175H}$/HLA-A*02:01 with a dissociation constant (K_d) of 86 nM, an association rate constant (k_{on}) of $1.76 \times 10^5\ M^{-1}\ s^{-1}$, and a dissociation rate constant (k_{off}) of $1.48 \times 10^{-2}\ s^{-1}$ (Fig. 1B). The k_{on} of $1.76 \times 10^5\ M^{-1}\ s^{-1}$ suggested a lack of overall conformational

Author Manuscript Author Manuscript Author Manuscript Author Manuscript

change of the $p53^{R175H}$/HLA-A*02:01 upon binding (31). No detectable binding of the H2-scDb to $p53^{WT}$/HLA-A*02:01 was observed in the SPR experiments (Fig. 1B).

Next, we examined whether anti-CD3 arms of the scDb other than the original UCHT1 could influence the ability of H2 to induce T cell activation. We linked the H2-scFv to a panel of commonly used anti-$CD3_\varepsilon$ scFvs, including UCHT1 (32), UCHT1v9 (33), L2K-07 (34), OKT3 (35), and hXR32 (36) (fig. S3A). We found that among the anti-$CD3_\varepsilon$ scFvs tested, UCHT1, which has the highest reported affinity (table S3), activated T cells at the lowest $p53^{R175H}$ peptide concentration when linked to the H2-scFv (Fig. 1C and fig. S3B). H2-UCHT1-scDb (hereafter, H2-scDb) was thus used for further experiments. Thermal stability of the purified H2-scDb as measured with differential scanning fluorimetry (DSF) showed a single melting temperature (T_m) at 69°C, suggesting that it is a stable molecule (fig. S3, C and D).

H2-scDb specifically recognizes cancer cells expressing the $p53^{R175H}$ neoantigen

We next evaluated the ability of H2-scDb to recognize cancer cell lines that express various amounts of HLA-A*02:01 and have different p53 mutation status. H2-scDb elicited T cell responses in a dose-dependent manner when T cells were cocultured with four cell lines that expressed moderate to high amounts of HLA-A*02:01 and harbored $p53^{R175H}$ (KMS26, KLE, TYK-nu, as well as the cisplatin-resistant variant of TYK-nu) (Fig. 2, A and B, and fig. S4A). This activation was noted even at very low (subnanomolar) concentrations of the bispecific antibody and was strictly T cell– and H2-scDb–dependent (fig. S4, B and C). The T cell responses resulted in potent killing of target cells and were polyfunctional, as indicated by the release of cytotoxic granule proteins granzyme B and perforin as well as the production of cytokines IFN-γ, tumor necrosis factor α (TNF-α), interleukin-2 (IL-2), and others (Fig. 2C and fig. S4, C to F). Clustering of T cells around tumor cells, leading to their lysis in the presence of H2-scDb, was also visualized with real-time live-cell imaging (Fig. 2D and movie S1). The requirement for both the $p53^{R175H}$ peptide and HLA-A*02:01 was evident from the observation that much lower amounts of IFN-γ were induced by cells harboring a $p53^{R175H}$ mutation but with low expression of HLA-A*02:01 (AU565 or SK-BR3) or by cells without $p53^{R175H}$ but with relatively high expression of HLA-A*02:01 (Fig. 2B and fig. S5A).

We further validated the specificity of H2-scDb using nine pairs of isogenic cell lines that differed with respect to HLA-A*02:01 expression or $p53^{R175H}$ mutation (Fig. 3A). First, we transfected human embryonic kidney (HEK) 293FT (*TP53*^{WT}/HLA-A*02:01) or Saos-2 (*TP53*^{null}/HLA-A*02:01) cells with plasmids that express either full-length $p53^{WT}$ or $p53^{R175H}$. H2-scDb induced robust T cell activation when cocultured with both cell lines overexpressing $p53^{R175H}$ but not with $p53^{WT}$-overexpressing or parental cells (Fig. 3B). Second, we transduced HLA-A*02:01-expressing retrovirus into four cell lines (AU565, SK-BR-3, HuCCT1, and CCRF-CEM) that harbored the $p53^{R175H}$ mutation but had low expression of HLA-A*02:01 (fig. S5B). Exogenous expression of HLA-A*02:01 in all four lines conferred T cell activation mediated by H2-scDb (Fig. 3C). Third, we genetically disrupted *TP53* in KMS26, KLE, and TYK-nu cancer cell lines that carry endogenous HLA-A*02:01 and $p53^{R175H}$, using a CRISPR-based technology (fig. S6A). T cell activation, as

Author Manuscript Author Manuscript Author Manuscript Author Manuscript

assessed from IFN-γ secretion, was reduced to control levels when *TP53* was disrupted in all three cell lines (Fig. 3D). The cytotoxicity mediated by H2-scDb was similarly mitigated by the disruption of *TP53* in these cells (Fig. 3E and fig. S6B).

Overall structure of the H2-Fab-p53^{R175H}/HLA-A*02:01 ternary complex

To understand the structural basis for the high specificity of the H2 clone for p53^{R175H}/HLA-A*02:01, we first converted H2 into a full-length immunoglobulin G (IgG) (H2-IgG) and confirmed that binding specificity was preserved in this format (fig. S7A). The H2-IgG was then digested into an antigen-binding fragment (H2-Fab) with papain (fig. S7B). The H2-Fab-p53^{R175H}/HLA-A*02:01 complex was purified (fig. S7, C and D), and its crystal structure was determined through molecular replacement and refined to 3.5 Å resolution [Protein Data Bank (PDB) ID 6W51] (table S4). There were four H2-Fab and four p53^{R175H}/HLA-A*02:01 per asymmetric unit (Fig. 4, A and B), with a pairwise root-mean-square deviation (RMSD) ranging from 0.27 to 0.45 Å for 382 to 419 C^{α} carbons, as calculated with PyMOL (table S5). All four H2-Fab were firmly positioned on the p53^{R175H}/HLA-A*02:01 with a total buried surface area of the interface calculated as 1173 Å^2, with roughly equal contributions from heavy and light chains (644 and 529 Å^2, respectively) (table S6) (37). Although the entire structure was refined to a resolution of 3.5 Å, particularly clear electron densities were observed for the p53^{R175H} peptide, the complementarity-determining regions (CDRs) of the H2-Fab, and the HLA-A*02:01 (Fig. 4, C and D). Viewed from the axis of the C terminus to the N terminus of the p53^{R175H} peptide, the CDRs were arranged in the order H2, H1, L3, H3, L1, and L2 (Fig. 4, E, F, and G). The docking angle of the H2-Fab to the p53^{R175H}-pHLA was 36° (Fig. 4, G and H). This orientation angle was quite different from those of most previously described TCRs or TCRm antibodies to pHLA complexes, in which the axis of the peptide is almost perpendicular to the axis defined between the disulfide bonds of the V_L/α to V_H/β chains (fig. S8).

Binding of the p53^{R175H} peptide to HLA-A*02:01

The p53^{R175H} peptide (HMTEVVRHC) occupied the binding cleft α1-α2 of HLA-A*02:01, burying a solvent-accessible surface area of 870 Å^2, which is slightly larger than other peptide/HLA-A*02:01 complexes (Fig. 5, A and B, and fig. S9A) and with the C-terminal arginine at position 7 (Arg^{174}) and mutant histidine at position 8 (His^{175}) pointing up, out of the groove. By contrast, the N terminus of the peptide is situated deep within the peptide-binding cleft, anchored by multiple residues in the HLA-A*02:01 (Fig. 5, A and B, and fig. S9A). The anchor residues of the peptide, a methionine at position 2 (P2; Met^{169}) and a cysteine residue at position 9 (P9; Cys^{176}) (fig. S9B), departed from the canonical anchor residues, leucine at P2 and valine or leucine at P9 (38). Peptides that bind to HLA-A*02:01 through either a methionine at P2 or a cysteine at P9 have been reported, but not both (39, 40). On the basis of alignments with structures of other HLA-A*02:01 peptides in complex with TCR or TCRm, the unconventional anchoring of p53^{R175H} did not result in drastic peptide conformational change or positioning (fig. S9, C and D).

Author Manuscript Author Manuscript Author Manuscript Author Manuscript

Structural basis for the recognition of p53^{R175H}/HLA-A*02:01 by the H2-Fab

The recognition of the HLA-A*02:01 by the H2-Fab was mediated by all six CDRs. There were a total of 79 contacts, with a cutoff of 4 Å, between the H2-Fab CDRs and the α1 and α2 helices of HLA-A*02:01, with the light chain contributing to 61% of those contacts (table S6). The H2-Fab buried a solvent-accessible surface area of 818 Å^2 within the HLA, of which 427 Å^2 were contributed by the light chain and 391 Å^2 by the heavy chain (table S6). By contrast, only four of the six H2-Fab CDRs (H1, H2, H3, and L3) interacted with the p53^{R175H} peptide. Overall, the H2-Fab made 36 contacts with the p53^{R175H} peptide, including five hydrogen bonds and numerous van der Waals interactions. His^{175} made 47% of all direct contacts with the H2-Fab. The CDR-H1, -H2, and -H3 of the heavy chain and CDR-L3 of the light chain formed a cage-like configuration around the C terminus of the p53^{R175H} peptide, trapping Arg^{174} and His^{175} into position by providing a stable interaction (Fig. 5C). The imidazole side chain of His^{175} was anchored by a hydrogen-bonding network with Asp^{54} (CDR-H2) and Tyr^{94} (CDR-L3) (Fig. 5C and fig. S10). Tyr^{52} (CDR-H2) acted as a ceiling and capped the cage-like structure around His^{175} by forming π-π interactions (Fig. 5C and fig. S10).

Assessing candidate cross-reactive peptides

One of the major challenges confronting new immunotherapeutic antibodies is off-target binding, which can result in toxicity to normal cells. Several powerful approaches to profile TCR and TCRm specificity have been developed to address this important issue (41-44). We used scanning mutagenesis to identify peptides in the human proteome with which H2-scDb might cross-react (44). A peptide library was generated by systemically substituting amino acids at each position of the target p53^{R175H} peptide (HMTEVVRHC) with each of the remaining 19 common amino acids (44). T2 cells loaded with each of the 171 variant peptides were then used to assess T cell activation by measuring IFN-γ release after incubation with T cells and H2-scDb (Fig. 5D). In congruence with the x-ray structural analysis, any changes in P8, where the mutant histidine residue lies, and any change in P7, which is encased with P8 by the CDR loops, abolished recognition of the peptide by H2-scDb. Peptides with substitutions at these positions retained their ability to bind to HLA-A*02:01 (fig. S11A). Other nonanchor residues at positions 3 to 6 also highly favored the parental amino acids present in the target peptide. This recognition pattern is illustrated as a Seq2Logo graph (Fig. 5E).

Next, we generated a nonamer binding motif, x-[ILMVNQTC]-[ST]-[DE]-[IV]-[IMVST]-R-H-[AILVGHSTYC], using 20% target peptide reactivity as a cutoff for permissive amino acids at each position (fig. S11B). A search of this motif in the UniProtKB human protein database by using ScanProsite (45) yielded three homologous peptides from signal transducer and activator of transcription 2 (STAT2) (PLTEIIRHY), vacuolar protein sorting 13 homolog A (VPS13A) (LQSEVIRHY), and zinc finger protein 3 (ZFP3) (QNSEIIRHI) (table S7). None of these three peptides were predicted to be potent binders of HLA-A*02:01 by NetMHCpan 4.0 (percent rank all >2.0) and had lower predicted binding affinity than that of the parental p53^{R175H} peptide (table S7) (25). However, to experimentally exclude the possibility of cross-reactivity, we pulsed T2 cells with each of these peptides. H2-scDb activated T cells only in the presence of T2 cells pulsed with the p53^{R175H} peptide

Author Manuscript Author Manuscript Author Manuscript Author Manuscript

(Fig. 5F). Additionally, we cotransfected COS-7 cells with expression plasmids for HLA-A*02:01 and full-length STAT2 or ZFP3; VPS13A was not tested because of its large size (>3000 amino acids). Again, no T cell activation was detected in the coculture assay with COS-7 cells expressing the two proteins that contain the candidate cross-reactive peptides (fig. S11, C and D).

Antitumor activity of the H2-scDb in vivo

To determine whether H2-scDb could control tumor growth in vivo, we engrafted KMS26 multiple myeloma cells into NOD-SCID-/*Il2rg*$^{-/-}$ (NSG) mice through intravenous injection, establishing widespread, actively growing cancers throughout the body. We used two models to assess the effects of the H2-scDb in combination with human T cells engrafted in these mice (Fig. 6, A and B, and fig. S12A). In an early treatment model, mice were randomized according to luminescence quantification of tumor burden, and H2-scDb was subsequently administered through continuous intraperitoneal infusion pumps at 0.3 mg/kg/day, starting 1 day after tumor inoculation. The pumps were able to maintain detectable plasma concentrations of scDb for 2 weeks (fig. S12B). An irrelevant isotype scDb was administered to mice in parallel as control. H2-scDb markedly suppressed the growth of parental KMS26 tumors (Fig. 6A). By contrast, the H2-scDb had no effect on KMS26 tumors in which the *TP53* gene had been disrupted by use of CRISPR (Fig. 6A). In the second model, mice were treated 6 days after tumor inoculation. The H2-scDb was administered at two doses (0.15 and 0.3 mg/kg/day). Both doses resulted in major tumor regressions and were well tolerated as assessed by the absence of changes in body weight (Fig. 6B and fig. S12C). No treatment effect of H2-scDb was observed in the absence of human T cells, supporting the T cell–dependent nature of H2-scDb (fig. S12D).

Discussion

The results described in this manuscript establish several important principles. First, it is possible to develop an antibody fragment (the H2-scFv) that specifically recognizes the protein product of an inactivated tumor suppressor gene and does not recognize the WT form in intact cells. The gene product is intracellular—largely located within the nucleus—and the recognition is made possible by the binding of the peptide derived from the mutant protein to a common HLA allele expressed on the cell surface. Second, the antibody is not only specific to the mutant form of the protein but appears not to comparably recognize any other peptide in the human peptidome. Third, a bispecific antibody constructed from H2 (H2-scDb) can activate T cells even when the pHLA complex is expressed at very low, endogenous levels. Fourth, the H2-scDb induces polyfunctional T cell effector responses, including cytotoxic activity and the production of multiple cytokines, which are likely the basis for its antitumor activities in vivo.

There have been no previous crystal structures of a TCRm antibody bound to a mutation-associated neoantigen complexed with HLA, and the structure reported here provides insights into the specificity of the H2-Fab fragment. Cancer-driver mutations often result in single-amino acid substitutions at mutation hotspots. pHLAs derived from such mutations differ from their WT counterparts only by one amino acid; thus, neoantigen-specific TCRm

Author Manuscript Author Manuscript Author Manuscript Author Manuscript

antibodies must be able to discern this subtle but critical difference. The specificity of the H2 antibody fragment was conferred by the extensive interaction of all the heavy chain CDR loops and one light chain CDR loop with the C-terminal residues of the $p53^{R175H}$ peptide, centering on the mutant histidine residue His^{175}. Both the mutant residue His^{175} and the adjacent residue Arg^{174} protruding out of the α1-α2 HLA helices increased the available recognition surface compared with other HLA-A*02:01 pHLA complexes, in which only one bulky residue is the central motif for recognition. Lack of recognition of the WT peptide by the H2 antibody fragment is likely due to the arginine residue at position 8 colliding with the "ceiling" of the cage-like structure of H2 (specifically a tyrosine at CDR-H2 amino acid 52) that surrounds the neoantigen mutation His^{175}. The binding of the H2-Fab also showed selectivity at positions 3 to 6, which was conferred through numerous van der Waals interactions with CDRs H3 and L3. Our findings also indicate that TCRm antibodies can bind to the HLA perpendicular to the typically diagonal TCRm orientation, strengthening the notion that there are no exclusive modes of recognition for pHLA by antibodies (40, 46, 47).

Targeting tumor-associated pHLA antigens is often confronted by the challenge of low antigen density (48). Neoantigen pHLAs are present in a few to a few dozen copies per cell based on MS quantification of multiple cancer cell lines (27). On the basis of our MS analysis, H2-scDb appears to recognize cancer cells that present endogenous neoantigens at single-digit quantities, which is comparable with native TCRs and affinity-matured soluble TCR bispecific antibodies (48, 49). Additionally, H2-scDb is able to react to its target antigen at considerably lower densities compared with what was reported for BiTEs, the format used in blinatumomab (50). There are several factors that could account for the reactivity of H2-scDb, including the particular scDb format we used here, intrinsic properties of the antibody and its mode of binding to the pHLA (for example, the cage-like structure stabilizing the interactions with the neoantigen mutation His^{175}), or the particular high-affinity anti-$CD3_\varepsilon$ scFv chosen after testing several others. In addition, the initial recognition of pHLA by H2-scDb induces T cell IFN-γ release, which might in turn up-regulate pHLA expression of adjacent cells in a feedforward process (51). Regardless, our results suggest that it is possible to effectively target pHLA complexes that are present at very low densities on the cell surface, offering promise for the creation of scDbs that recognize the epitopes of proteins encoded by other mutant driver genes.

Naturally occurring human TCRs have undergone thymic selection that limits their potential to cross-react with normal tissues. For engineered TCRs, cross-reactivity to similar peptides potentially present in the human peptidome is a serious concern because such cross-reactivity has resulted in fatal toxicities (52, 53). Comprehensive prediction of the on-target off-tumor activity of TCR and TCRm has proven to be challenging (52). In this work, we used a previously suggested strategy to screen for potential off-tumor peptide targets by first establishing the recognition motif and then searching the human peptidome for peptides that conform to this motif (44). We thereby identified three homologous peptides, but no binding to H2 was evident when any of these peptides were evaluated with the same techniques used to assess the $p53^{R175H}$ peptide. However, these experiments cannot entirely exclude the possibility of off-tumor reactivity, which can only be addressed through formal toxicity testing in nonhuman primates and eventually in human clinical trials.

Author Manuscript Author Manuscript Author Manuscript Author Manuscript

TCR- and TCRm-based bispecific antibodies have been developed to target aberrantly expressed—but not mutated—intracellular oncogenic and tumor-associated antigens (TAAs) such as Wilms tumor 1 (WT1), gp100, MAGE-A3, Melan-A, and NY-ESO-1 (15, 48). By contrast, adoptive cell therapy has been used to target pHLA derived from not only intracellular TAAs and WT oncogenes but also mutant oncogenes and tumor suppressor genes (8, 16, 54, 55). Although adoptive cell therapy has been remarkably successful in some patients, its widespread implementation is constrained by the need for patients' autologous cells and for sophisticated manipulation of the cells in an individualized manner (16). The same is true for CAR-T cells, which have resulted in long-term remissions and perhaps even cures in patients with B cell leukemias and lymphomas (18-20). Protein-based therapies are advantageous over cell-based therapies in that they can be "off-the-shelf," are considerably easier to manufacture, and much less expensive (56).

We have shown that it is possible to develop an antibody-based therapeutic that targets the most common mutation of the most commonly mutated tumor suppressor gene in human cancers. This therapeutic agent appears to be exquisitely specific to cancer cells harboring the mutation. The research described here represents an essential first step in the long journey to developing an agent that is based on the H2-scDb that could be successfully used to treat cancer patients.

Materials and methods

Cell lines and primary T cells

COS-7, RPMI 6666, Jurkat, T2 (174 x CEM.T2), Raji, HH, AU565, SK-BR-3, KLE, HCT116, SW480, NCI-H441, NCI-H358, A-427, Saos-2, and CCRF-CEM cells were purchased from American Type Culture Collection (ATCC). KMS26, TYK-nu, TYK-nu.CP-r, and HuCCT1 were purchased from Japanese Collection of Research Bioresources Cell Bank (JCRB). SigM5 was obtained from DSMZ. HEK293FT was obtained from Invitrogen (Thermo Fisher Scientific). T2, Raji, Jurkat, HH, AU565, NCI-H441, NCI-H358, CCRF-CEM, KMS26, TYK-nu, TYK-nu.CP-r, and HuCCT1 were cultured in RPMI-1640 (ATCC, 30-2001) with 10% FBS (GE Healthcare, SH30070.03) and 1% penicillin-streptomycin (Thermo Fisher Scientific, 15140163). RPMI 6666 was cultured in RPMI-1640 with 20% FBS and 1% penicillin-streptomycin. A-427 was cultured in Eagle's Minimum Essential Medium (ATCC, 30-2003) with 10% FBS and 1% penicillin-streptomycin. COS-7, SK-BR-3, HCT116, SW480, and Saos-2 were cultured in McCoy's 5A modified medium (Thermo Fisher Scientific, 16600108) with 10% FBS and 1% penicillin-streptomycin. SigM5 was cultured in IMDM (Thermo Fisher Scientific, 12440061) with 20% FBS and 1% penicillin-streptomycin. HEK293FT was cultured in DMEM (high glucose, pyruvate, Thermo Fisher Scientific, 11995065) with 10% FBS, additional 2 mM GlutaMAX (Thermo Fisher Scientific, 35050061), 0.1 mM MEM non-essential amino acids (Thermo Fisher Scientific, 11140050), 1% penicillin-streptomycin, and 500 μg/ml Geneticin (Thermo Fisher Scientific, 10131027). PBMCs were isolated from leukapheresis samples (Stem Cell Technologies) by standard density gradient centrifugation with Ficoll Paque Plus (GE Healthcare, 17144003). T cells were expanded from PBMCs with addition of the anti-human CD3 antibody (OKT3, BioLegend, 317347) at 15 ng/ml for three days. T cells were cultured

Author Manuscript Author Manuscript Author Manuscript Author Manuscript

in RPMI-1640 with 10% FBS, 1% penicillin-streptomycin, 100 IU/ml recombinant human IL-2 (aldesleukin, Prometheus Therapeutics and Diagnostics), and 5 ng/ml recombinant human IL-7 (BioLegend, 581908). In general, T cells from at least one male and one female donor were tested in in vitro assays. All cells were grown at 37°C in 5% CO_2 with humidification.

Detection of $p53^{R175H}$ peptide

HLA-A*02:01 restricted $p53^{R175H}$ peptide was directly detected and quantified through MANA-SRM in COS-7 cells transfected with HLA-A*02:01 and $p53^{R175H}$ and in human cancer cells carrying $p53^{R175H}$ mutations and expressing HLA-A*02:01 (27). The dual-reduction approach described in MANA-SRM was critical for this detection because a cysteine and a methionine coexist in the $p53^{R175H}$ peptide. One hundred femtomoles of heavy-isotope labeled $p53^{R175H}$ peptide HMTEVVRHC and $p53^{WT}$ peptide HMTEVVRRC (New England Peptide) were spiked into each sample before the assay. The MANA-SRM assays were performed at Complete Omics.

Peptides and monomers

All peptides were synthesized at a purity of >90% by Peptide 2.0 or ELIM Biopharm, except for the positional scanning library, where crude peptides were used. Peptides were resuspended in dimethylformamide at 10 mg/ml and stored at −20°C. Biotinylated pHLA monomers were synthesized by Fred Hutchinson Cancer Research Center Immune Monitoring Lab. Monomers were confirmed to be folded by performing an ELISA using W6/32 antibody (BioLegend, 311402), which recognizes only folded HLA (57).

Phage display library construction

The scFv-bearing phage library used in this study has been described in detail previously (28). Briefly, oligonucleotides were synthesized by GeneArt (Thermo Fisher Scientific) using trinucleotide mutagenesis (TRIM) technology to diversify complementarity-determining region (CDR)-L2, CDR-L3, CDR-H1, CDR-H2, and CDR-H3. A FLAG (DYKDDDDK) epitope tag was placed immediately downstream of the scFv, which was followed in-frame by the full-length M13 pIII coat protein sequence. The total number of transformants obtained was determined to be 3.6×10^{10}.

Selection of mutant pHLA specific phage clone

Phage clones bearing scFvs specific to $p53^{R175H}$/HLA-A*02:01 pHLA were identified using the general approach previously described (58). One μg of biotinylated HLA-A*02:01 pHLA monomer complexes were conjugated to 50 μl of M-280 streptavidin magnetic Dynabeads (Thermo Fisher Scientific, 11206D). During the enrichment phase (Round 1), phages were negatively selected with a mixture of unconjugated Dynabeads and free streptavidin protein (RayBiotech, 228-11469). After negative selection, supernatant containing unbound phages was transferred for positive selection using 1 μg of $p53^{R175H}$/HLA-A*02:01 pHLA. Beads were then washed and phages were eluted to infect mid-log-phase SS320 bacteria, with the addition of M13K07 helper phages (multiplicity of infection

Author Manuscript Author Manuscript Author Manuscript Author Manuscript

of 4). Bacteria were then grown overnight at 30°C for phage production, and the phages were precipitated the next morning with PEG/NaCl.

During the selection phase (Rounds 2-5), phages from the previous round were subjected to two stages of negative selection: (i) against cell lines without $p53^{R175H}$/HLA-A*02:01 (RPMI 6666, Jurkat, Raji, SigM5, HH, T2, NCI-H441, NCI-H358, A-427, and COS-7) and (ii) against $p53^{WT}$/HLA-A*02:01 pHLA, unrelated HLA-A*02:01 pHLA, and free streptavidin. For negative selection using cell lines, phages were incubated with a total number of 5×10^8 to 1×10^9 of cells at 4°C overnight. After negative selection, beads were isolated and unbound phages were transferred for positive selection by incubating with 1 μg (Round 2), 0.5 μg (Round 3), or 0.25 μg (Rounds 4 and 5) of $p53^{R175H}$/HLA-A*02:01 pHLA. Phages were then eluted and amplified by infecting SS320 as described above.

After five rounds of selection, SS320 cells were infected with a limiting dilution of the enriched phages. A total of 190 individual colonies of SS320 were picked, and phage DNA was PCR amplified by primers flanking the CDRs (Forward: GGCCATGGCAGATATTCAGA, Reverse: CCGGGCCTTTATCATCATC) using Q5 Hot Start High-Fidelity 2X Master Mix (New England BioLabs, M0494L) and Sanger sequenced by GENEWIZ. Sequences flanking the CDRs were trimmed using DNA Baser Sequence Assembler v4 (Heracle BioSoft), and the sequences spanning the CDRs were clustered using the CD-HIT Suite (59). Colonies containing unique phage clones were selected and grown overnight in 400 μl of media in deep 96-well plates (Thermo Fisher Scientific, 278743) with the addition of M13K07 helper phages. Bacteria were pelleted the next day, and the phage-laden supernatants were used for downstream analysis.

Peptide pulsing

For peptide pulsing, T2 cells were washed with serum-free RPMI-1640 medium before incubation at 0.5×10^6 to 1×10^6 cells per ml in serum-free RPMI-1640 containing peptides at the specified concentration for 2 hours at 37°C. For experiments using flow cytometry, human β2M (ProSpec, PRO-337) at 10 μg/ml was added with the peptides and specified in the figure legends of such experiments.

Flow cytometry

Phage staining of peptide-pulsed T2 cells was performed with 50 μl phage supernatant on ice for 1 hour, followed by staining with 1 μg of rabbit anti-M13 antibody (Novus Biologicals, NB100-1633) and PE anti-rabbit IgG (BioLegend, 406421). HLA-A*02 staining was performed by staining cells with APC-labeled anti-human HLA-A*02 (BB7.2, BioLegend, 343308) or mouse isotype IgG2b, κ (BioLegend, 402206). Human T cells engrafted in mice were stained with Brilliant Violet (BV) 421 anti-human CD3 (SK7, BioLegend, 344834) and BV605 anti-human CD8(SK1, BioLegend, 344742). Stained cells were analyzed using an LSRII flow cytometer (Becton Dickinson) or an iQue Screener (IntelliCyt).

Author Manuscript Author Manuscript Author Manuscript Author Manuscript

ELISAs

Streptavidin-coated 96-well plates (R&D Systems, CP004) were coated with 50 ng of biotinylated HLA-A*02:01 pHLA monomers in 50 μl of blocking buffer (PBS with 0.5% BSA, 2 mM EDTA, and 0.1% sodium azide) or 25 ng of recombinant human $CD3_{\varepsilon}/\delta$ (Acro Biosystems, CDD-H82W6) at 4°C overnight. Plates were washed with 1X TBST (TBS + 0.05% Tween-20) using a BioTek 405 TS plate washer. Serial dilutions of scDb or IgG were incubated on plates for 1 hour at room temperature (RT) and washed. For scDbs, the plate was then incubated with 1 μg/ml recombinant protein L (Thermo Fisher Scientific, 77679) for 1 hour at RT, washed, followed by incubation with antiprotein L HRP (1:10000, Abcam, ab63506) for 1 hour at RT. For IgG, the plate was incubated with anti-human IgG HRP (1:1000, Thermo Fisher Scientific, 62-8420) for 1 hour at RT. Plates were washed, 50 μl of 3,3′,5,5′-Tetramethylbenzidine (TMB) substrate (BioLegend, 421101) was added to each well, and the reaction was quenched with 50 μl 1N sulfuric acid (Thermo Fisher Scientific, SA212-1). Absorbance at 450 nm was measured with a Synergy H1 Multi-Mode Reader (BioTek).

scDb production

scDbs were produced by cloning gBlocks (IDT) encoding each of the variants in the format (from N- to C terminus): IL-2 signal sequence, anti-pHLA variable light chain (V_L), GGGGS short linker, anti-CD3 variable heavy chain (V_H), $(GGGGS)_3$ long linker, anti-CD3 V_L, GGGGS short linker, anti-pHLA V_H, and 6 x HIS tag into linearized pcDNA3.4 vector (Thermo Fisher Scientific, A14697). The proteins were expressed by the Eukaryotic Tissue Culture Core Facility of Johns Hopkins University. Briefly, 1 mg of plasmid DNA was transfected with polyethylenimine (PEI) at a ratio of 1:3 into 1L of FreeStyle 293-F cells at a concentration of 2×10^6 to 2.5×10^6 cells per ml, and the transfected cells were incubated at 37°C. Five days after transfection, culture medium was collected and filtered through a 0.2 μm vacuum filter system (Corning, 09-761-107). The scDbs were purified using HisPur Ni-NTA Resin (Thermo Fisher Scientific, 88222) and desalted into PBS pH 7.4 or 20 mM Tris pH 9.0, 150 mM NaCl using 7k MWCO Zeba Spin desalting columns (Thermo Fisher Scientific, 89890). Proteins were quantified using a 4 to 15% Mini-PROTEAN TGX gel (Bio-Rad, 4568085) and/or NanoDrop (Thermo Fisher Scientific). Alternatively, the scDb proteins were produced by GeneArt (Thermo Fisher Scientific) in Expi293, purified with a HisTrap column (GE Healthcare, 17525501) followed by size exclusion chromatography with a HiLoad Superdex 200 16/600 column (GE Healthcare, 28989335). Analytic chromatography was performed using TSKgel G3000SWxl column (TOSOH Bioscience) using a running buffer of 50 mM sodium phosphate and 300 mM sodium chloride at pH 7, at a flow rate of 1.0 ml/min.

Surface plasmon resonance affinity measurements of $p53^{R175H}$/HLA-A*02:01 and H2-scDb interaction

Biotinylated $p53^{R175H}$/HLA-A*02:01, $p53^{WT}$/HLA-A*02:01, and H2-scDb binding experiments were performed at 25°C using a Biacore T200 SPR instrument (GE Healthcare). Approximately 100 to 110 response units (RU) of biotinylated $p53^{R175H}$/HLA-A*02:01 and $p53^{WT}$/HLA-A*02:01 were captured in flow cells (Fc) 2 and 4, respectively,

Author Manuscript Author Manuscript Author Manuscript Author Manuscript

using a streptavidin chip. Single-cycle kinetics were performed by injecting increasing concentrations (3, 12, 50, 200, and 800 nM) of purified H2-scDb, which was flowed over Fc 1-4. Binding responses for kinetic analysis were both blank- and reference-subtracted (60). Both binding curves were fit with a 1:1 binding model using Biacore Insight evaluation software.

Differential scanning fluorimetry

Thermal stability of the H2-scDb was evaluated by a differential scanning fluorimetry (DSF) assay, which monitors the fluorescence of a dye that binds to the hydrophobic region of a protein as it becomes exposed upon temperature-induced denaturation (61-63). Reaction mixture (20 μl) was set up in a white low-profile 96-well, unskirted polymerase chain reaction plate (BioRad, MLL9651) by mixing 2 μl of purified H2-scDb at a concentration of 1 mg/ml (final concentration 0.1 mg/ml) with 2 μl of 50X SYPRO orange dye (Invitrogen, S6650, 5X final concentration) in PBS, pH 7.4. The plate was sealed with an optical transparent film (Thermo Fisher Scientific, 4311971) and centrifuged for 1,000 x *g* for 30 s. Thermal scanning was performed from 25 to 100°C (1°C/min temperature gradient) using a CFX9 Connect real-time polymerase chain reaction instrument (BioRad). Protein unfolding/melting temperature T_m was calculated from the maximum value of the negative first derivative of the melt curve using CFX Manager software (BioRad).

CRISPR-mediated knockout of TP53

The Alt-R CRISPR system (IDT) was used to knock out the *TP53* gene from KMS26, TYK-nu, and KLE cell lines. CRISPR-Cas9 crRNAs targeting *TP53* exon 3 (p53-5: CCCCGGACGATATTGAACAA or p53-6: CCCCTTGCCGTCCCAAGCAA) as well as CRISPR-Cas9 tracrRNA were resuspended at 100 μM with Nuclease-Free Duplex Buffer. The crRNAs and tracrRNA were duplexed at a 1:1 molar ratio for 5 min at 95°C followed by cooling down slowly to RT according to the manufacturer's instructions. The duplexed RNA was then mixed with Cas9 Nuclease at a 1.2:1 molar ratio for 15 min. A total of 40 pmol of the Cas9 RNP complexed with *TP53* gRNA were mixed with 2×10^5 cells in 20 μl of OptiMEM. This mixture was loaded into a 0.1 cm cuvette (Bio-Rad, 1652089) and electroporated at 120 V and 16 ms using an ECM 2001 (BTX). Cells were transferred to complete growth medium and cultured for 7 days. Single cell clones were established by limiting dilution and genomic DNA was harvested using a Quick-DNA 96 Kit (Zymo Research, D3012). A region flanking the CRISPR cut site was PCR-amplified (forward primer: GCTGCCCTGGTAGGTTTTCT, reverse primer: GAGACCTGTGGGAAGCGAAA) and Sanger sequenced to select for clones with the desired *TP53* status.

Immunoblotting analysis

Cells were lysed in cold RIPA buffer (Thermo Fisher Scientific, 89901) supplemented with protease inhibitor cocktail (Thermo Fisher Scientific, 87785). Protein concentration was determined using a BCA assay (Thermo Fisher Scientific, 23227). Equal amounts of total protein (20 to 50 μg) were loaded in each lane of a 4 to 15% Mini-PROTEAN TGX gel (Bio-Rad, 4568085) and transferred to polyvinylidene difluoride membranes after electrophoresis. The membranes were incubated with appropriate primary antibodies

Author Manuscript Author Manuscript Author Manuscript Author Manuscript

[anti-6x His tag, 1:2000, Abcam, ab9108; p53 (DO-1), 1:1000, Santa Cruz, sc-126; STAT2, 1:1000, Thermo Fisher Scientific, 44-362G; ZFP3, 1:1000, Thermo Fisher Scientific, PA5-62726; β-actin (13E5), 1:1000, Cell Signaling Technology, 5125S; β-actin (8H10D10), 1:1000, Cell Signaling Technology, 3700S] and species-specific HRP-conjugated secondary antibodies (1:5000-10000). Signal was detected by a ChemiDoc MP chemiluminescence system (Bio-Rad).

Transfection of cell lines

gBlocks (IDT) encoding HLA and target proteins were cloned into pcDNA3.1 or pcDNA3.4 vectors (Thermo Fisher Scientific, V79020, A14697). COS-7, HEK293FT, and Saos-2 cells were transfected at 70 to 80% confluency using Lipofectamine 3000 (Thermo Fisher Scientific, L3000015) and incubated at 37°C overnight. A total of 15 μg and 30 μg plasmid (1:1 ratio of HLA plasmid/target protein plasmid in co-transfections) was used for T25 and T75 flasks, respectively.

Viral transduction of cell lines

HLA-A*02:01-encoding retrovirus was produced using the MSCV retroviral expression system (Clontech, 634401). In brief, a gBlock encoding HLA-A*02:01-T2A-GFP (IDT) was cloned into the pMSCVpuro retroviral vector by HiFi DNA assembly (New England Biolabs, E2621L). The pMSCVpuro-HLA-A*02:01-T2A-GFP plasmid was then co-transfected with a pVSV-G envelope vector into the GP2-293 packaging cell line (Clontech, 631530). Viral supernatant was harvested 48 hours after transfection and concentrated 20-fold using Retro-X Concentrator (Clontech, 631456). RediFect Red-Fluc-GFP lentivirus particles (Perkin Elmer, CLS960003) was used for generating luciferase-expressing cell lines. NucLight green lentivirus (Essen Bioscience, 4624) was used to generate TYK-nu cell lines with nuclear GFP expression.

For transduction, non-tissue culture-treated 48-well plates were coated with 200 μl of 10 μg/ml RetroNectin (Clontech, T100B) per well overnight at 4°C and blocked with 10% FBS for 1 hour at RT. Viral particles and 2×10^5 target cells were added to each well in a total volume of 500 μl cell culture medium and centrifuged at 2000 × g for 1 hour then incubated at 37°C. Selection with 1 μg/ml puromycin (Thermo Fisher Scientific, A1113803) began three days later. Transduced cells were sorted based on presence of GFP using FACSAria Fusion (BD Biosciences) 10 to 14 days after transduction.

In vitro scDb co-incubation assays

In each well of a 96-well flat-bottom plate, the following components were combined in a final volume of 100 μl RPMI-1640 with 10% FBS, 1% penicillin-streptomycin, and 100 IU/ml IL-2: scDb diluted to the specified concentration, 5×10^4 human T cells, and 1×10^4 to 5×10^4 target cells (COS-7, T2, or other tumor cell lines). The effector to target cell ratio is specified in the figure legend for each experiment. The coculture plate was incubated for 20 hours at 37°C, and conditioned medium was assayed for cytokine and cytotoxic granule protein secretion using the Human IFN-γ Quantikine Kit (R&D Systems, SIF50), Human IFN-γ Flex Set Cytometric Bead Array (BD, 558269), or the MILLIPLEX Luminex assays (Millipore Sigma, HSTCMAG28SPMX13, HCD8MAG-15K) read on the Bioplex 200

Author Manuscript Author Manuscript Author Manuscript Author Manuscript

platform (Bio-Rad). Cytotoxicity was assayed by CellTiter-Glo Luminescent Cell Viability Assay (Promega, G7571), Bio-Glo Luciferase Assay (Promega, G7941), or Steady-Glo Luciferase Assay (Promega, E2510) per manufacturer's instructions. For CellTiter-Glo assays, percent cytotoxicity was calculated by subtracting the luminescence signal from the average of the T cell only wells and normalizing to the no scDb condition: [1 – (scDb well – T cell only)/(no scDb well – T cell only)] × 100. For Bio-Glo and Steady-Glo assays, percent cytotoxicity was calculated by normalizing luminescence signal to the no scDb condition: [1 – (scDb well)/(no scDb well)] × 100.

Real-time live-cell imaging

A total of 1×10^4 NucLight Green-labeled target cells were plated in each well of a 96-well flat bottom plate and allowed to attach for 4 hours before adding 2×10^4 or 5×10^4 T cells and scDb at the indicated concentrations. Each condition was plated in triplicate. Plates were imaged every 3 hours using the IncuCyte ZOOM Live-Cell analysis system (Essen Bioscience) for a total of 120 hours. Four images per well at 10X zoom were collected at each time point. The number of GFP-positive objects per mm^2 in each well was quantified using the green fluorescence channel.

Expression, purification, and refolding of $p53^{R175H}$/HLA-A*02:01

Plasmids for HLA-A*02:01 and β2M were received from the NIH Tetramer Facility and separately transformed into BL21(DE3) cells. Each was expressed in inclusion bodies using auto-induction medium as previously described (64-66). Purification of the HLA-A*02:01 and β2M inclusion bodies was achieved with a series of detergent washes followed by solubilization with 8 M urea. Refolding of the HLA-A*02:01, β2M, and mutant $p53^{R175H}$ peptide was performed as previously described (28). Briefly, solubilized HLA-A*02:01 and β2M were combined in a refolding buffer containing 100 mM Tris pH 8.3, 400 mM L-arginine, 2 mM EDTA, 5 mM reduced glutathione, 0.5 mM oxidized glutathione, 2 mM PMSF, and 30 mg of the mutant $p53^{R175H}$ peptide (amino acids 168 to 176, HMTEVVRHC) dissolved in ml of DMSO. The resultant solution was stirred at 4°C for 2 days, with two further additions of HLA-A*02:01 on day 2, concentrated to 10 ml, and purified by size exclusion chromatography on a HiLoad 26/60 Superdex 75 Prep grade column (GE Healthcare, 28989334). For incubation with the H2-Fab, purified pHLA-A*02:01 was concentrated to ~1 to 3 mg/ml and stored at −80°C until use.

Production of the H2-Fab antibody fragment

The light chain (LC) and heavy chain (HC) variable region sequences of H2 scFv were grafted onto the respective constant chains of trastuzumab and separately cloned into a pcDNA3.4 vector (Thermo Fisher Scientific, A14697). Both chains were preceded by a mouse IgKVIII signal peptide. Before large-scale expression of full-length antibody, optimization of the LC:HC DNA ratio for transfection was performed to determine optimal recombinant protein yields. For a 1 L expression, 1 mg of purified plasmids (1:1 LC:HC ratio) were transfected with PEI at a ratio of 1:3 into Freestyle 293-F cells at a concentration of 2×10^6 to 2.5×10^6 cells per ml and incubated at 37°C for 7 days. The medium was harvested via centrifugation, filtered through a 0.22-μm PES membrane, and the full-length antibody was purified via protein A affinity chromatography on a HiTrap MabSelect SuRe

Author Manuscript Author Manuscript Author Manuscript Author Manuscript

column (GE Healthcare, 29049104). Full-length antibody was eluted using a linear gradient of 0 to 100 mM sodium citrate, pH 3.5. The protein A fractions containing pure H2 antibody were pooled, quantified by SDS-PAGE gel electrophoresis, and dialyzed into 20 mM sodium phosphate buffer, pH 7.0, 10 mM EDTA.

For generation of H2-Fab fragments, ~1 to 3 mg of full-length antibody was mixed with 0.5 ml of a 50% Immobilized Papain slurry (Thermo Fisher Scientific, 20341) pre-activated with digestion buffer (20 mM sodium phosphate buffer, pH 7.0, 10 mM EDTA) containing 20 mM cysteine-HCl. The mixture was incubated at 37°C overnight with constant shaking at 200 rpm. The H2 antibody digest was separated from the immobilized resin by a gravity resin separator and washed with 10 mM Tris-HCl, pH 7.5. Newly generated H2-Fab fragments were further purified by cation-exchange chromatography using a Mono-S column (GE Healthcare, 17516801) and eluted using a linear gradient of 0 to 500 mM NaCl.

The H2-Fab fragments were concentrated, mixed with equimolar $p53^{R175H}$/HLA-A*02:01, and incubated at 4°C overnight. The H2-Fab–$p53^{R175H}$/HLA-A*02:01 mixture was evaluated by size exclusion chromatography on a Superdex 200 Increase 10/300 column (GE Healthcare, 28990944). The fractions of ~ 98% pure pHLA-A*02:01-H2-Fab complex were pooled, concentrated to 12.6 mg/ml, and exchanged into a buffer containing 25 mM HEPES, pH 7.0, 200 mM NaCl.

Crystallization, data collection, and structure determination

Crystals of the ternary complex H2-Fab–$p53^{R175H}$/HLA-A*02:01 were grown by vapor diffusion in hanging drops set up with a TTP mosquito robot with a reservoir solution of 0.2 M ammonium chloride and 20% (w/v) PEG 3350 MME. Crystals were flash-cooled in mother liquor. Data were collected at National Synchrotron Light Source-II at beamlines 17-ID-1(AMX) on a Dectris EIGER X 16M detector. The dataset was indexed, integrated, and scaled using fastdp (67), XDS (68), and aimless (69). Monoclinic crystals of H2-Fab–$p53^{R175H}$/HLA-A*02:01 diffracted to 3.5 Å. The structure for the H2-Fab-$p53^{R175H}$/HLA-A*02:01 complex was determined by molecular replacement with PHASER (70) using PDB ID 6O4Y (71) and 6UJ9 as the search models. The data were refined to a final resolution of 3.5 Å using iterative rounds of refinement with REFMAC5 (72, 73) and manual rebuilding in Coot (74). Structures were validated using Coot and PDB Deposition tools. The model has 95.2% of the residues in preferred and 3.8% in allowed regions according to Ramachandran statistics (table S4). Figures were rendered in PyMOL (v2.2.3, Schrödinger, LLC). Buried areas were calculated with PDBePISA (37). The docking angle that determines the relative orientation between the pHLA and the Fab/TCR was calculated by the web server TCR3d (75, 76).

Mouse xenograft model

Female NOD.*Cg-Prkdc*^{scid}*Il2rg*^{tm1Wjl}/SzJ (NSG) mice at 6 to 10 weeks were acquired from the Jackson Laboratory (005557) and treated in compliance with the institutional Animal Care and Use Committee approved protocol (Protocol #M018M79). In the early treatment model, mice were inoculated intravenously with 1×10^6 luciferase-expressing KMS26 or *TP53* KO KMS26 cells and 1×10^7 in vitro expanded human T cells via lateral tail vein

Author Manuscript Author Manuscript Author Manuscript Author Manuscript

injection on day 0. On day 1, mice were randomized based on luminescence quantification using the IVIS imaging system and Living Image software (Perkin Elmer) to ensure similar pretreatment tumor burden. Prior to imaging, mice received intraperitoneal injection of luciferin (150 μl, RediJect D-Luciferin Ultra Bioluminescent Substrate, PerkinElmer, 770505) and were anesthetized using inhaled isoflurane in an induction chamber for 5 min. After randomization, two-week micro-osmotic pumps (ALZET, 1002) filled with H2-scDb, isotype control scDb (scFv against an irrelevant pHLA linked with UCHT1 scFv), or vehicle only that had been primed in 1 ml PBS overnight at 37°C were placed intraperitoneally using sterile surgical technique. Tumor growth was serially monitored by bioluminescent imaging. In the established tumor model, mice were inoculated with 3.5×10^5 or 5×10^5 luciferase-expressing KMS26 cells and 1×10^7 human T cells via lateral tail vein injection on day 0. On day 6, H2-scDb or isotype control scDb was administered similarly as in the early treatment model. The number of mice included in each arm was determined by the maximal number of intraperitoneal pump placement surgery that could be carried out in a given experiment.

For mouse blood-based analysis, 200 μl blood was collected in EDTA-treated microvettes (Sarstedt, 20.1278.100) by cheek bleed, followed by centrifugation at 1000 x g for 3 min. Plasma was collected and stored at −80°C until analysis. The blood cell pellet was resuspended with 100 μl PBS, followed by two 5-min incubations with 1 ml ACK lysis buffer (Thermo Fisher Scientific, A1049201) with one PBS wash in between, and resuspended in flow stain buffer with TruStain FcX (anti-mouse CD16/32) antibody (BioLegend, 101320) and cell-surface staining antibodies as indicated in the text. For scDb quantification, plasma was thawed and incubated in biotinylated recombinant human CD3ε/δ coated streptavidin plate and detected as described under ELISAs.

Statistical analysis

Data are presented as means ± SD unless otherwise specified. Statistical analyses were carried out using specific tests indicated in the figure legends. A P value of <0.05 was used to denote statistical significance unless specifically indicated. All analyses were performed using Prism version 8.0 (GraphPad).

Supplementary Material

Refer to Web version on PubMed Central for supplementary material.

ACKNOWLEDGMENTS

The expression of antibodies and single-chain diabodies was carried out at the Eukaryotic Tissue Culture Facility of the Johns Hopkins University School of Medicine. The plasmids for expression of HLA-A*02:01 and β_2-microglobulin were a gift from the NIH Tetramer Core Facility (Emory University, Atlanta, California). The authors acknowledge the help of B. G. Pierce and R. Gowthaman for tailoring the web server TCR3d for antibodies. We thank S. Sur, N. Wyhs, A. Cook, M. Dal Molin, R. L. Blosser, A. Tam, L. Dasko-Vincent, C. Thoburn, J. Rodríguez Molina, and J. Cao for assistance with this study. The illustrations were created with https://BioRender.com.

Funding:

This work was supported by the Virginia and D. K. Ludwig Fund for Cancer Research, the Lustgarten Foundation for Pancreatic Cancer Research, the Commonwealth Fund, the Bloomberg~Kimmel Institute for Cancer Immunotherapy, Bloomberg Philanthropies, the Mark Foundation for Cancer Research, and NIH Cancer Center

Author Manuscript Author Manuscript Author Manuscript Author Manuscript

support grant P30 CA006973. J.D., B.J.M., A.H.P., and S.R.D. were supported by NIH grant T32 GM73009. S.P. was supported by NIH grant 5T32 CA009071-38 and SITC-Amgen Cancer Immunotherapy in Hematologic Malignancies Fellowship. M.F.K. was supported by NIH grant T32 AR048522. C.B. was supported by NCI grant R37 CA230400. Work at the AMX (17-ID-1) and FMX (17-ID-2) beamlines was supported by the NIH, the National Institute of General Medical Sciences (P41GM111244), the U.S. Department of Energy (DOE) Office of Biological and Environmental Research (KP1605010), and the National Synchrotron Light Source II at Brookhaven National Laboratory, which is supported by the DOE Office of Basic Energy Sciences under contract DE-SC0012704 (KC0401040).

REFERENCES AND NOTES

1. Alexandrov LB et al., Signatures of mutational processes in human cancer. Nature 500, 415–421 (2013). doi: 10.1038/nature12477; pmid: 23945592 [PubMed: 23945592]
2. Vogelstein B et al., Cancer genome landscapes. Science 339, 1546–1558 (2013). doi: 10.1126/science.1235122; pmid: 23539594 [PubMed: 23539594]
3. Garraway LA, Lander ES, Lessons from the cancer genome. Cell 153, 17–37 (2013). doi: 10.1016/j.cell.2013.03.002; pmid: 23540688 [PubMed: 23540688]
4. Gerstung M et al., The evolutionary history of 2,658 cancers. Nature 578, 122–128 (2020). doi: 10.1038/s41586-019-1907-7; pmid: 32025013 [PubMed: 32025013]
5. Bouaoun L et al., TP53 Variations in Human Cancers: New Lessons from the IARC TP53 Database and Genomics Data. Hum. Mutat 37, 865–876 (2016). doi: 10.1002/humu.23035; pmid: 27328919 [PubMed: 27328919]
6. Hollstein M, Sidransky D, Vogelstein B, Harris CC, p53 mutations in human cancers. Science 253, 49–53 (1991). doi: 10.1126/science.1905840; pmid: 1905840 [PubMed: 1905840]
7. Malekzadeh P et al., Neoantigen screening identifies broad TP53 mutant immunogenicity in patients with epithelial cancers. J. Clin. Invest 129, 1109–1114 (2019). doi: 10.1172/JCI123791; pmid: 30714987 [PubMed: 30714987]
8. Lo W et al., Immunologic recognition of a shared p53 mutated neoantigen in a patient with metastatic colorectal cancer. Cancer Immunol. Res 7, 534–543 (2019). doi: 10.1158/2326-6066.CIR-18-0686; pmid: 30709841 [PubMed: 30709841]
9. Grossman RL et al., Toward a shared vision for cancer genomic data. N. Engl. J. Med 375, 1109–1112 (2016). doi: 10.1056/NEJMp1607591; pmid: 27653561 [PubMed: 27653561]
10. González-Galarza FF et al., Allele frequency net 2015 update: New features for HLA epitopes, KIR and disease and HLA adverse drug reaction associations. Nucleic Acids Res. 43 (D1), D784–D788 (2015). doi: 10.1093/nar/gku1166; pmid: 25414323 [PubMed: 25414323]
11. Dao T et al., Targeting the intracellular WT1 oncogene product with a therapeutic human antibody. Sci. Transl. Med 5, 176ra33 (2013). doi: 10.1126/scitranslmed.3005661; pmid: 23486779
12. Chang AY et al., A therapeutic T cell receptor mimic antibody targets tumor-associated PRAME peptide/HLA-I antigens. J. Clin. Invest 127, 2705–2718 (2017). doi: 10.1172/JCI92335; pmid: 28628042 [PubMed: 28628042]
13. Li D et al., Development of a T-cell receptor mimic antibody against wild-type p53 for cancer immunotherapy. Cancer Res. 77, 2699–2711 (2017). doi: 10.1158/0008-5472.CAN-16-3247; pmid: 28363997 [PubMed: 28363997]
14. Low L, Goh A, Koh J, Lim S, Wang C-I, Targeting mutant p53-expressing tumours with a T cell receptor-like antibody specific for a wild-type antigen. Nat. Commun 10, 5382 (2019). doi: 10.1038/s41467-019-13305-z; pmid: 31772160 [PubMed: 31772160]
15. Dao T et al., Therapeutic bispecific T-cell engager antibody targeting the intracellular oncoprotein WT1. Nat. Biotechnol 33, 1079–1086 (2015). doi: 10.1038/nbt.3349; pmid: 26389576 [PubMed: 26389576]
16. Klebanoff CA, Rosenberg SA, Restifo NP, Prospects for gene-engineered T cell immunotherapy for solid cancers. Nat. Med 22, 26–36 (2016). doi: 10.1038/nm.4015; pmid: 26735408 [PubMed: 26735408]
17. Rafiq S et al., Optimized T-cell receptor-mimic chimeric antigen receptor T cells directed toward the intracellular Wilms Tumor 1 antigen. Leukemia 31, 1788–1797 (2017). doi: 10.1038/leu.2016.373; pmid: 27924074 [PubMed: 27924074]

Author Manuscript Author Manuscript Author Manuscript Author Manuscript

18. Maude SL et al., Chimeric antigen receptor T cells for sustained remissions in leukemia. N. Engl. J. Med 371, 1507–1517 (2014). doi: 10.1056/NEJMoa1407222; pmid: 25317870 [PubMed: 25317870]
19. Park JH et al., Long-Term Follow-up of CD19 CAR Therapy in acute lymphoblastic leukemia. N. Engl. J. Med 378, 449–459 (2018). doi: 10.1056/NEJMoa1709919; pmid: 29385376 [PubMed: 29385376]
20. Schuster SJ et al., Tisagenlecleucel in adult relapsed or refractory diffuse large B-cell lymphoma. N. Engl. J. Med 380, 45–56 (2019). doi: 10.1056/NEJMoa1804980; pmid: 30501490 [PubMed: 30501490]
21. Robbins PF et al., A pilot trial using lymphocytes genetically engineered with an NY-ESO-1-reactive T-cell receptor: Long-term follow-up and correlates with response. Clin. Cancer Res 21, 1019–1027 (2015). doi: 10.1158/1078-0432.CCR-14-2708; pmid: 25538264 [PubMed: 25538264]
22. Rafiq S, Hackett CS, Brentjens RJ, Engineering strategies to overcome the current roadblocks in CAR T cell therapy. Nat. Rev. Clin. Oncol 17, 147–167 (2020). doi: 10.1038/s41571-019-0297-y; pmid: 31848460 [PubMed: 31848460]
23. Labrijn AF, Janmaat ML, Reichert JM, Parren PWHI, Bispecific antibodies: A mechanistic review of the pipeline. Nat. Rev. Drug Discov 18, 585–608 (2019). doi: 10.1038/s41573-019-0028-1; pmid: 31175342 [PubMed: 31175342]
24. Kantarjian H et al., Blinatumomab versus chemotherapy for advanced acute lymphoblastic leukemia. N. Engl. J. Med 376, 836–847 (2017). doi: 10.1056/NEJMoa1609783; pmid: 28249141 [PubMed: 28249141]
25. Andreatta M, Nielsen M, Gapped sequence alignment using artificial neural networks: Application to the MHC class I system. Bioinformatics 32, 511–517 (2016). doi: 10.1093/bioinformatics/btv639; pmid: 26515819 [PubMed: 26515819]
26. Parkhurst MR et al., Unique neoantigens arise from somatic mutations in patients with gastrointestinal cancers. Cancer Discov. 9, 1022–1035 (2019). doi: 10.1158/2159-8290.CD-18-1494; pmid: 31164343 [PubMed: 31164343]
27. Wang Q et al., Direct detection and quantification of neoantigens. Cancer Immunol. Res 7, 1748–1754 (2019). doi: 10.1158/2326-6066.CIR-19-0107; pmid: 31527070 [PubMed: 31527070]
28. Miller MS et al., An engineered antibody fragment targeting mutant β-catenin via major histocompatibility complex I neoantigen presentation. J. Biol. Chem 294, 19322–19334 (2019). doi: 10.1074/jbc.RA119.010251; pmid: 31690625 [PubMed: 31690625]
29. Douglass J et al., Bispecific antibodies targeting mutant, neoantigens. Sci. Immunol 6, eabd5515 (2021). [PubMed: 33649101]
30. Paul S et al., TCR beta chain-directed bispecific antibodies for the treatment of T cell cancers. Sci. Transl. Med 10.1126/scitranslmed.abd3595 (2021).
31. Wu H et al., Kinetic and structural analysis of mutant CD4 receptors that are defective in HIV gp120 binding. Proc. Natl. Acad. Sci. U.S.A 93, 15030–15035 (1996). doi: 10.1073/pnas.93.26.15030; pmid: 8986758 [PubMed: 8986758]
32. Beverley PC, Callard RE, Distinctive functional characteristics of human “T” lymphocytes defined by E rosetting or a monoclonal anti-T cell antibody. Eur. J. Immunol 11, 329–334 (1981). doi: 10.1002/eji.1830110412; pmid: 6788570 [PubMed: 6788570]
33. Zhu Z, Lewis GD, Carter P, Engineering high affinity humanized anti-p185HER2/anti-CD3 bispecific F(ab’)2 for efficient lysis of p185HER2 overexpressing tumor cells. Int. J. Cancer 62, 319–324 (1995). doi: 10.1002/ijc.2910620315; pmid: 7628874 [PubMed: 7628874]
34. Dreier T et al., Extremely potent, rapid and costimulation-independent cytotoxic T-cell response against lymphoma cells catalyzed by a single-chain bispecific antibody. Int. J. Cancer 100, 690–697 (2002). doi: 10.1002/ijc.10557; pmid: 12209608 [PubMed: 12209608]
35. Van Wauwe JP, De Mey JR, Goossens JG, OKT3: A monoclonal anti-human T lymphocyte antibody with potent mitogenic properties. J. Immunol 124, 2708–2713 (1980). pmid: 6966296 [PubMed: 6966296]
36. Huang L, Johnson LS, CD3-binding molecules capable of binding to human and non-human CD3. Macrogenics (2014).

Author Manuscript Author Manuscript Author Manuscript Author Manuscript

37. Krissinel E, Henrick K, Inference of macromolecular assemblies from crystalline state. J. Mol. Biol 372, 774–797 (2007). doi: 10.1016/j.jmb.2007.05.022; pmid: 17681537 [PubMed: 17681537]
38. Sarkizova S et al., A large peptidome dataset improves HLA class I epitope prediction across most of the human population. Nat. Biotechnol 38, 199–209 (2020). doi: 10.1038/s41587-019-0322-9; pmid: 31844290 [PubMed: 31844290]
39. Webb AI et al., Functional and structural characteristics of NY-ESO-1-related HLA A2-restricted epitopes and the design of a novel immunogenic analogue. J. Biol. Chem 279, 23438–23446 (2004). doi: 10.1074/jbc.M314066200; pmid: 15004033 [PubMed: 15004033]
40. Ataie N et al., Structure of a TCR-mimic antibody with target predicts pharmacogenetics. J. Mol. Biol 428, 194–205 (2016). doi: 10.1016/j.jmb.2015.12.002; pmid: 26688548 [PubMed: 26688548]
41. Gejman RS et al., Identification of the targets of T-cell receptor therapeutic agents and cells by use of a high-throughput genetic platform. Cancer Immunol. Res 8, 672–684 (2020). doi: 10.1158/2326-6066.CIR-19-0745; pmid: 32184297 [PubMed: 32184297]
42. Kula T et al., T-Scan: A genome-wide method for the systematic discovery of T cell epitopes. Cell 178, 1016–1028. e13 (2019). doi: 10.1016/j.cell.2019.07.009; pmid: 31398327 [PubMed: 31398327]
43. Coles CH et al., TCRs with distinct specificity profiles use different binding modes to engage an identical peptide-HLA complex. J. Immunol 204, 1943–1953 (2020). doi: 10.4049/jimmunol.1900915; pmid: 32102902 [PubMed: 32102902]
44. Harper J et al., An approved in vitro approach to preclinical safety and efficacy evaluation of engineered T cell receptor anti-CD3 bispecific (ImmTAC) molecules. PLOS ONE 13, e0205491 (2018). doi: 10.1371/journal.pone.0205491; pmid: 30321203 [PubMed: 30321203]
45. de Castro E et al., ScanProsite: Detection of PROSITE signature matches and ProRule-associated functional and structural residues in proteins. Nucleic Acids Res. 34, W362–5 (2006). doi: 10.1093/nar/gkl124; pmid: 16845026 [PubMed: 16845026]
46. Stewart-Jones G et al., Rational development of high-affinity T-cell receptor-like antibodies. Proc. Natl. Acad. Sci. U.S.A 106, 5784–5788 (2009). doi: 10.1073/pnas.0901425106; pmid: 19307587 [PubMed: 19307587]
47. Raman MC et al., Direct molecular mimicry enables off-target cardiovascular toxicity by an enhanced affinity TCR designed for cancer immunotherapy. Sci. Rep 6, 18851 (2016). doi: 10.1038/srep18851; pmid: 26758806 [PubMed: 26758806]
48. Liddy N et al., Monoclonal TCR-redirected tumor cell killing. Nat. Med 18, 980–987 (2012). doi: 10.1038/nm.2764; pmid: 22561687 [PubMed: 22561687]
49. Purbhoo MA, Irvine DJ, Huppa JB, Davis MM, T cell killing does not require the formation of a stable mature immunological synapse. Nat. Immunol 5, 524–530 (2004). doi: 10.1038/ni1058; pmid: 15048111 [PubMed: 15048111]
50. Stone JD, Aggen DH, Schietinger A, Schreiber H, Kranz DM, A sensitivity scale for targeting T cells with chimeric antigen receptors (CARs) and bispecific T-cell Engagers (BiTEs). OncoImmunology 1, 863–873 (2012). doi: 10.4161/onci.20592; pmid: 23162754 [PubMed: 23162754]
51. Dunn GP, Koebel CM, Schreiber RD, Interferons, immunity and cancer immunoediting. Nat. Rev. Immunol 6, 836–848 (2006). doi: 10.1038/nri1961; pmid: 17063185 [PubMed: 17063185]
52. Cameron BJ et al., Identification of a Titin-derived HLA-A1-presented peptide as a cross-reactive target for engineered MAGE A3-directed T cells. Sci. Transl. Med 5, 197ra103 (2013). doi: 10.1126/scitranslmed.3006034; pmid: 23926201
53. Morgan RA et al., Cancer regression and neurological toxicity following anti-MAGE-A3 TCR gene therapy. J. Immunother 36, 133–151 (2013). doi: 10.1097/CJI.0b013e3182829903; pmid: 23377668 [PubMed: 23377668]
54. Chapuis AG et al., T cell receptor gene therapy targeting WT1 prevents acute myeloid leukemia relapse post-transplant. Nat. Med 25, 1064–1072 (2019). doi: 10.1038/s41591-019-0472-9; pmid: 31235963 [PubMed: 31235963]
55. Tran E et al., T-cell transfer therapy targeting mutant KRAS in cancer. N. Engl. J. Med 375, 2255–2262 (2016). doi: 10.1056/NEJMoa1609279; pmid: 27959684 [PubMed: 27959684]

Author Manuscript Author Manuscript Author Manuscript Author Manuscript

56. Goebeler ME, Bargou RC, T cell-engaging therapies - BiTEs and beyond. Nat. Rev. Clin. Oncol 17, 418–434 (2020). doi: 10.1038/s41571-020-0347-5; pmid: 32242094 [PubMed: 32242094]
57. Jefferies WA, MacPherson GG, Expression of the W6/32 HLA epitope by cells of rat, mouse, human and other species: Critical dependence on the interaction of specific MHC heavy chains with human or bovine beta 2-microglobulin. Eur. J. Immunol 17, 1257–1263 (1987). doi: 10.1002/eji.1830170907; pmid: 2443365 [PubMed: 2443365]
58. Skora AD et al., Generation of MANAbodies specific to HLA-restricted epitopes encoded by somatically mutated genes. Proc. Natl. Acad. Sci. U.S.A 112, 9967–9972 (2015). doi: 10.1073/pnas.1511996112; pmid: 26216968 [PubMed: 26216968]
59. Huang Y, Niu B, Gao Y, Fu L, Li W, CD-HIT Suite: A web server for clustering and comparing biological sequences. Bioinformatics 26, 680–682 (2010). doi: 10.1093/bioinformatics/btq003; pmid: 20053844 [PubMed: 20053844]
60. Myszka DG, Improving biosensor analysis. J. Mol. Recognit 12, 279–284 (1999). doi: 10.1002/(SICI)1099-1352(199909/10)12:5<279::AID-JMR473>3.0.CO;2-3; pmid: 10556875 [PubMed: 10556875]
61. Niesen FH, Berglund H, Vedadi M, The use of differential scanning fluorimetry to detect ligand interactions that promote protein stability. Nat. Protoc 2, 2212–2221 (2007). doi: 10.1038/nprot.2007.321; pmid: 17853878 [PubMed: 17853878]
62. Ericsson UB, Hallberg BM, Detitta GT, Dekker N, Nordlund P, Thermofluor-based high-throughput stability optimization of proteins for structural studies. Anal. Biochem 357, 289–298 (2006). doi: 10.1016/j.ab.2006.07.027; pmid: 16962548 [PubMed: 16962548]
63. Cheng M et al., Successful engineering of a highly potent single-chain variable-fragment (scFv) bispecific antibody to target disialoganglioside (GD2) positive tumors. OncoImmunology 5, e1168557 (2016). doi: 10.1080/2162402X.2016.1168557; pmid: 27471647 [PubMed: 27471647]
64. Altman JD, Davis MM, MHC-peptide tetramers to visualize antigen-specific T cells. Curr. Protoc. Immunol 115, 17.13.11–17.13, 44 (2016). doi: 10.1002/cpim.14; pmid: 27801510 [PubMed: 27801510]
65. Garboczi DN, Hung DT, Wiley DC, HLA-A2-peptide complexes: Refolding and crystallization of molecules expressed in *Escherichia coli* and complexed with single antigenic peptides. Proc. Natl. Acad. Sci. U.S.A 89, 3429–3433 (1992). doi: 10.1073/pnas.89.8.3429; pmid: 1565634 [PubMed: 1565634]
66. Studier FW, Protein production by auto-induction in high density shaking cultures. Protein Expr. Purif 41, 207–234 (2005). doi: 10.1016/j.pep.2005.01.016; pmid: 15915565 [PubMed: 15915565]
67. Winter G, McAuley KE, Automated data collection for macromolecular crystallography. Methods 55, 81–93 (2011). doi: 10.1016/j.ymeth.2011.06.010; pmid: 21763424 [PubMed: 21763424]
68. Kabsch W, Xds. Acta Crystallogr. D Biol. Crystallogr 66, 125–132 (2010). doi: 10.1107/S0907444909047337; pmid: 20124692 [PubMed: 20124692]
69. Evans PR, Murshudov GN, How good are my data and what is the resolution? Acta Crystallogr. D Biol. Crystallogr 69, 1204–1214 (2013). doi: 10.1107/S0907444913000061; pmid: 23793146 [PubMed: 23793146]
70. McCoy AJ et al., Phaser crystallographic software. J. Appl. Crystallogr 40, 658–674 (2007). doi: 10.1107/S0021889807021206; pmid: 19461840 [PubMed: 19461840]
71. Mishto M et al., An in silico–in vitro pipeline identifying an HLA-A*02:01^{+} KRAS G12V^{+} spliced epitope candidate for a broad tumor-immune response in cancer patients. Front. Immunol 10, 2572 (2019). doi: 10.3389/fimmu.2019.02572; pmid: 31803176 [PubMed: 31803176]
72. Winn MD et al., Overview of the *CCP4* suite and current developments. Acta Crystallogr. D Biol. Crystallogr 67, 235–242 (2011). doi: 10.1107/S0907444910045749; pmid: 21460441 [PubMed: 21460441]
73. Murshudov GN, Vagin AA, Dodson EJ, Refinement of macromolecular structures by the maximum-likelihood method. Acta Crystallogr. D Biol. Crystallogr 53, 240–255 (1997). doi: 10.1107/S0907444996012255; pmid: 15299926 [PubMed: 15299926]
74. Emsley P, Lohkamp B, Scott WG, Cowtan K, Features and development of Coot. Acta Crystallogr. D Biol. Crystallogr 66, 486–501 (2010). doi: 10.1107/S0907444910007493; pmid: 20383002 [PubMed: 20383002]

Author Manuscript Author Manuscript Author Manuscript Author Manuscript

75. Gowthaman R, Pierce BG, TCR3d: The T cell receptor structural repertoire database. Bioinformatics 35, 5323–5325 (2019). doi: 10.1093/bioinformatics/btz517; pmid: 31240309 [PubMed: 31240309]

76. Pierce BG, Weng Z, A flexible docking approach for prediction of T cell receptor-peptide-MHC complexes. Protein Sci. 22, 35–46 (2013). doi: 10.1002/pro.2181; pmid: 23109003 [PubMed: 23109003]

Author Manuscript Author Manuscript Author Manuscript Author Manuscript

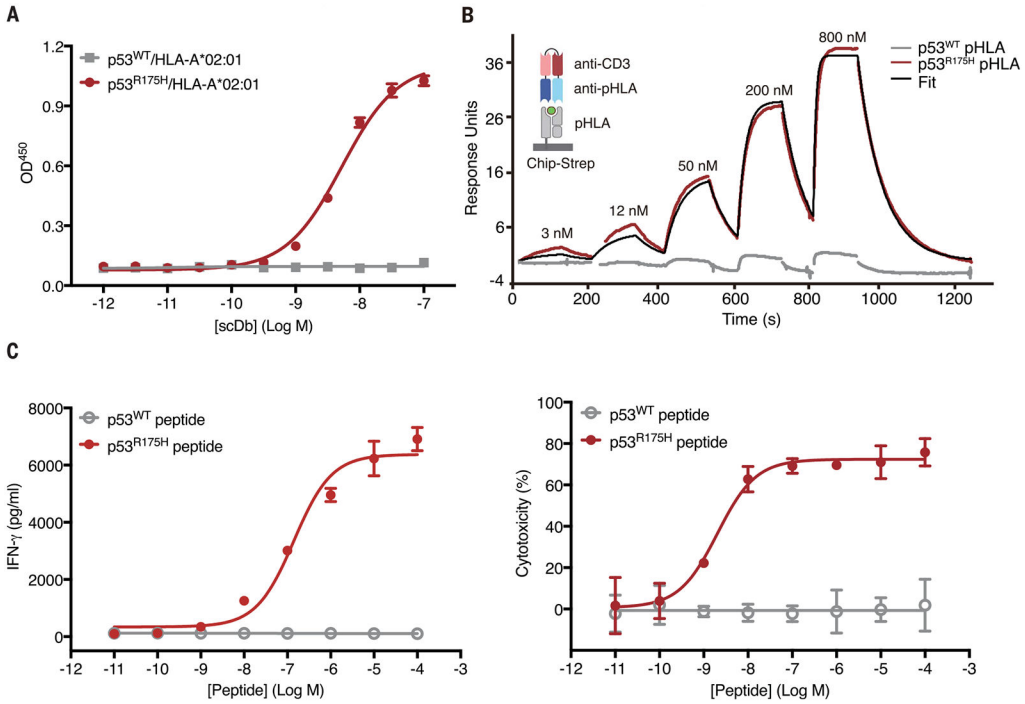

Fig. 1. Biological and biophysical characteristics of scFv clone H2.

(**A**) H2-scDb binding to immobilized p53^{R175H}/HLA-A*02:01 (red) or p53^{WT}/HLA-A*02:01 (gray) pHLA monomers was assessed by means of ELISA. Data shown represent mean ± SD of three technical replicates. (**B**) H2-scDb binding to p53^{R175H}/HLA-A*02:01 was measured with single-cycle kinetics by using SPR. H2-scDb was loaded at increasing concentrations. The blank- and reference-subtracted binding is shown for p53^{R175H}/HLA-A*02:01 (red) and p53^{WT}/HLA-A*02:01 (gray). H2-scDb binds to the p53^{R175H}/HLA-A*02:01 pHLA with one-to-one binding kinetics at a K_d of 86 nM (fitted black line). There was negligible p53^{WT}/HLA-A*02:01 binding. (**C**) T2 cells pulsed with p53^{WT} or p53^{R175H} peptide were co-incubated with 1 nM H2-scDb and T cells at an effector:target (E:T) ratio of 2:1. IFN-γ release was measured with ELISA (left), and cell lysis was evaluated by means of luminescent cytotoxicity assay (right). Data indicate mean ± SD of three technical replicates and are representative of three independent experiments.

Author Manuscript Author Manuscript Author Manuscript Author Manuscript

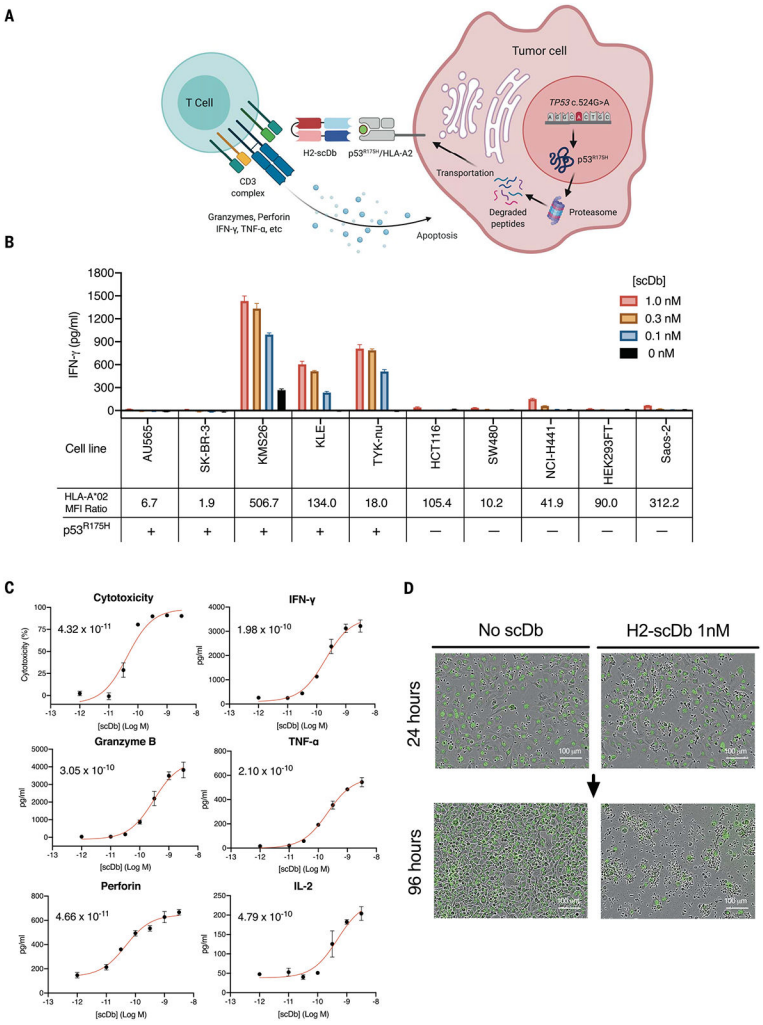

Fig. 2. H2-scDb activates T cells in the presence of tumor cells presenting p53^{R175H}.

(**A**) Illustration depicting the mechanism of action of H2-scDb. (**B**) HLA-A*02:01-positive tumor cell lines with different HLA expression and p53^{R175H} status were co-incubated with H2-scDb and T cells at an E:T ratio of 2:1. IFN-γ release was measured with ELISA. Data indicate mean ± SD of six technical replicates and are representative of two independent experiments. The HLA-A*02 MFI ratio is defined as MFI (anti-HLA-A*02)/MFI (isotype control). (**C**) Polyfunctional T cell activation mediated by H2-scDb in response to KMS26 at an E:T ratio of 2:1 was assessed from luminescent cytotoxicity and with antibody-based assays. Median effective concentration (EC_{50}) (M) for each assay is shown in the corresponding graph. Data indicate mean ± SD of three technical replicates and are representative of two independent experiments. (**D**) Real-time live-cell imaging of T cells co-incubated with green fluorescent protein (GFP)–labeled TYK-nu at an E:T ratio of 5:1 with or without H2-scDb. Representative phase contrast and green fluorescence images taken at 24 hours (top) and 96 hours (bottom) after mixing cells are shown.

Author Manuscript Author Manuscript Author Manuscript Author Manuscript

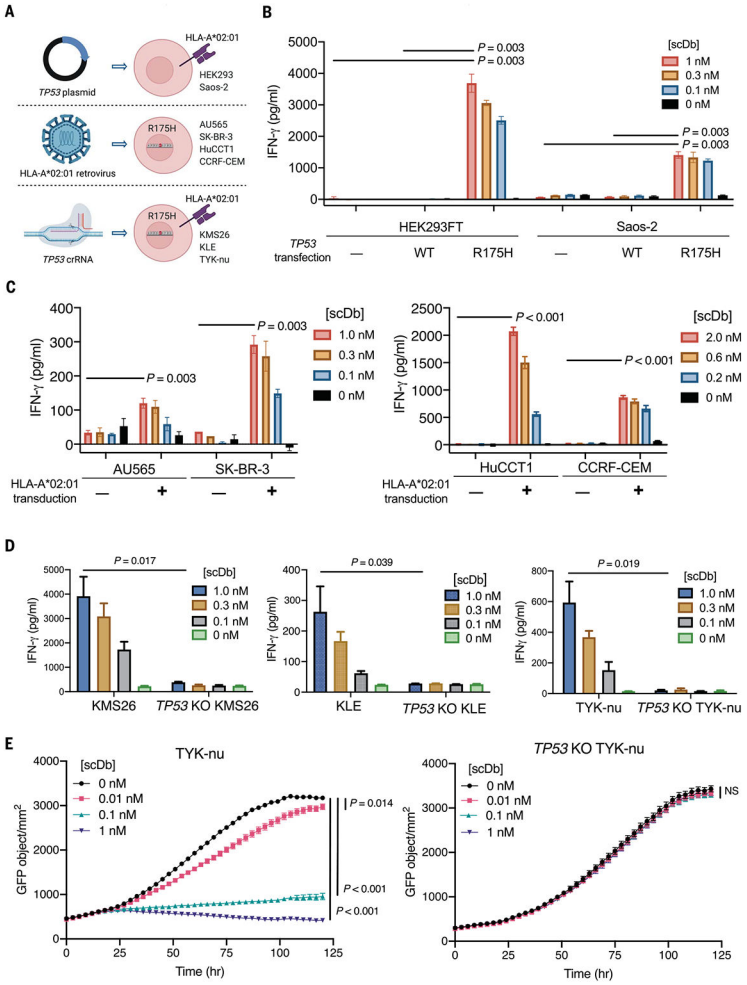

Fig. 3. Determination of H2-scDb specificity by using isogenic target cell lines.

(**A**) Methods of generating isogenic cell line pairs in cells with different HLA and *TP53* backgrounds. (**B**) HEK293FT and Saos-2 cell lines that were not transfected or were transfected with plasmids expressing either the full-length $p53^{WT}$ or full-length $p53^{R175H}$ were co-incubated with T cells at an E:T ratio of 1:1 (HEK293FT) or 2.5:1 (Saos-2) in the presence of increasing amounts of H2-scDb. IFN-γ release was measured with ELISA. Data indicate mean ± SD of three technical replicates and are representative of two independent experiments, analyzed by means of one-way analysis of variance (ANOVA) with Games-Howell multiple comparisons. (**C**) Cell lines expressing $p53^{R175H}$ and transduced or not transduced with a retrovirus expressing HLA-A*02:01 were co-incubated with H2-scDb and T cells at an E:T of 2:1. IFN-γ release was measured with ELISA. Data indicate mean ± SD of three technical replicates, analyzed by means of two-tailed *t* test. (**D**) H2-scDb-mediated IFN-γ release from T cells in response to parental tumor cell lines or their *TP53* KO counterparts at an E:T ratio of 2:1 was measured with ELISA. Data indicate mean ± SD of three technical replicates and are representative of two independent experiments, analyzed by means of two-tailed *t* test. (**E**) Parental (left) or *TP53* KO (right) TYK-nu cells labeled with nuclear GFP were co-incubated with H2-scDb and T cells at an E:T ratio of 2:1. Growth of TYK-nu cells was measured with real-time live-cell imaging. Data indicate mean

± SEM of 12 technical replicates, analyzed by means of two-tailed *t* test at the last time point, NS indicates no statistical significance comparing 0 nM scDb with each of the three scDb concentrations.

Author Manuscript Author Manuscript Author Manuscript Author Manuscript

Author Manuscript Author Manuscript Author Manuscript Author Manuscript

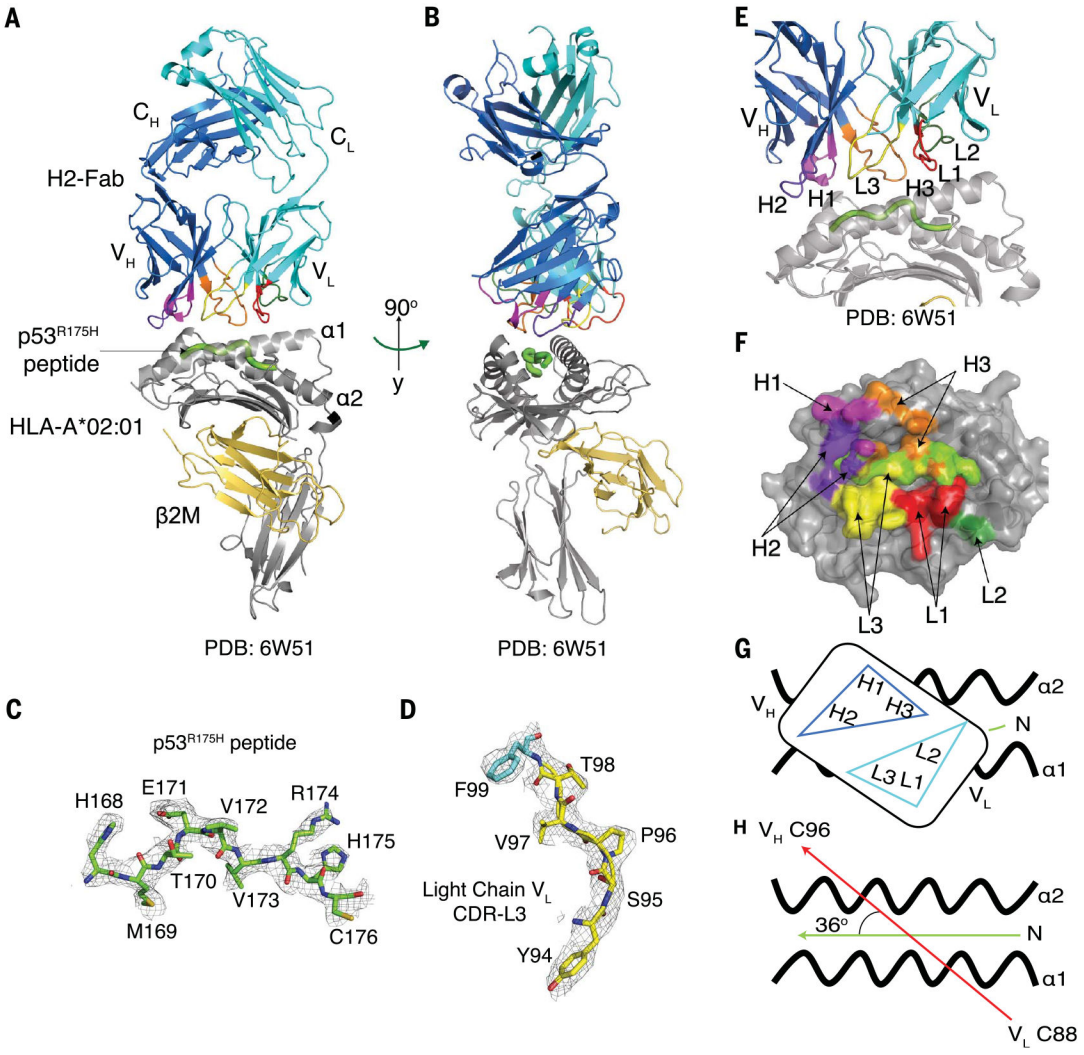

Fig. 4. H2-Fab binds to the HLA-A*02:01 and the C terminus of the p53^{R175H} peptide.

(**A**) Overall structure of p53^{R175H}/HLA-A*02:01 bound to the H2-Fab fragment (PDB ID 6W51). HLA-A*02:01 and β2 microglobulin (β2M) are colored in gray and gold, respectively. The H2-Fab is colored according to the heavy (blue) and light (cyan) chains of the Fab fragment. The p53^{R175H} nine–amino acid peptide is shown in light green between helices α1 and α2 of the HLA. (**B**) Structure of H2-Fab–p53^{R175H}/HLA-A*02:01 at 90° to that shown in (A). (**C**) Composite omit electron density map of the p53^{R175H} peptide contour at 1σ. (**D**) Composite omit electron density map of a selected area of the H2-Fab at CDR-L3 from residues 95 to 99 contoured at 1σ. (**E**) Zoomed-in view of the interaction of H2-Fab to p53^{R175H}/HLA-A*02:01 with CDRs colored as in (A). The CDRs are labeled and colored in order from left to right: H2 (purple), H1 (magenta), L3 (yellow), H3 (orange), L1 (red), L2 (dark green). (**F**) Bird's-eye view of surface representation of the HLA-A*02:01 shown in gray, p53^{R175H} peptide shown in light green, and the contacting residues colored according to CDRs of the H2-Fab as in (E). (**G**) Schematic representation of (F). (**H**) Diagram of the docking angle of the H2-Fab to p53^{R175H}/HLA-A*02:01. The docking angle is defined by two vectors: one from N to C termini of the peptide (green), and the other

between the C^{α} of Cys^{88} of the disulfide bond of the V_L domain and the C^{α} of Cys^{96} of the disulfide bond of the V_H domain of the H2-Fab (red). The arrowed lines indicate the direction of each vector. The docking angle was calculated by using the web server TCR3d (75, 76). Single-letter abbreviations for the amino acid residues are as follows: A, Ala; C, Cys; D, Asp; E, Glu; F, Phe; G, Gly; H, His; I, Ile; K, Lys; L, Leu; M, Met; N, Asn; P, Pro; Q, Gln; R, Arg; S, Ser; T, Thr; V, Val; W, Trp; and Y, Tyr.

Author Manuscript Author Manuscript Author Manuscript Author Manuscript

Author Manuscript Author Manuscript Author Manuscript Author Manuscript

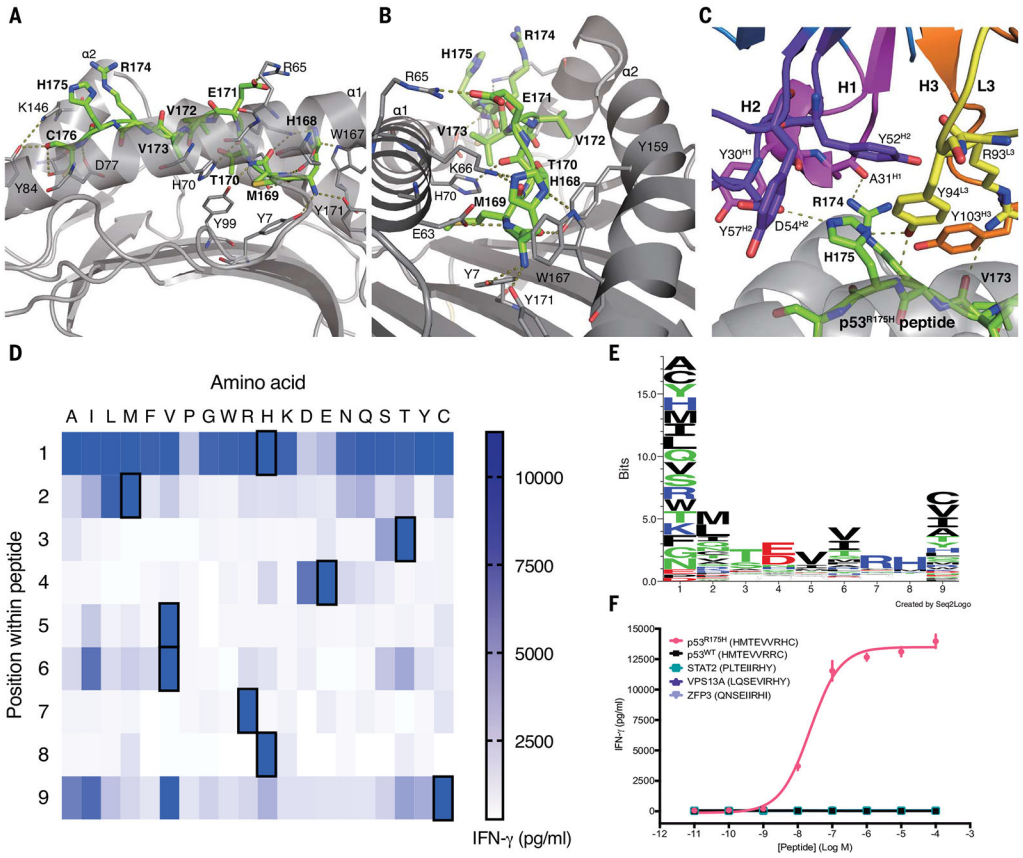

Fig. 5. Structural basis of H2 specificity and identification of putative cross-reactive peptides.

(**A**) Detailed interactions of the p53^{R175H} peptide with HLA-A*02:01. The peptide (green) and the side chains (gray) of interacting residues of HLA-A*02:01 are represented as sticks. Hydrogen bonds are shown as dashed lines. (**B**) Perpendicular view of the p53^{R175H} peptide binding cleft. (**C**) C terminus of the peptide (amino acids Val^{173} to Cys^{176}) with Arg^{174} and His^{175} surrounded by the interacting residues of CDR-H1 (magenta), -H2 (purple), -H3 (orange), and -L3 (yellow) shown as sticks. Hydrogen bonds are shown as dashed lines. (**D**) T2 cells were loaded with 10 μM HMTEVVRHC peptide variants from the positional scanning library and co-incubated with 1 nM H2-scDb and T cells at an E:T ratio of 2:1. IFN-γ release was measured with cytometric bead array, and the mean of duplicate wells was used to plot the heatmap. Black boxes indicate the amino acids in the parental p53^{R175H} peptide. (**E**) Illustration of the binding pattern of H2-scDb as Seq2Logo graph, calculated by dividing the IFN-γ value by 10^4 and using the PSSM-Logo algorithm. (**F**) T2 cells were loaded with 10 μM p53^{R175H}, p53^{WT}, STAT2, VPS13A, or ZFP3 peptide and co-incubated with 1 nM H2-scDb and T cells at an E:T ratio of 2:1. IFN-γ secretion was measured with ELISA. Data indicate mean ± SD of three technical replicates.

Author Manuscript Author Manuscript Author Manuscript Author Manuscript

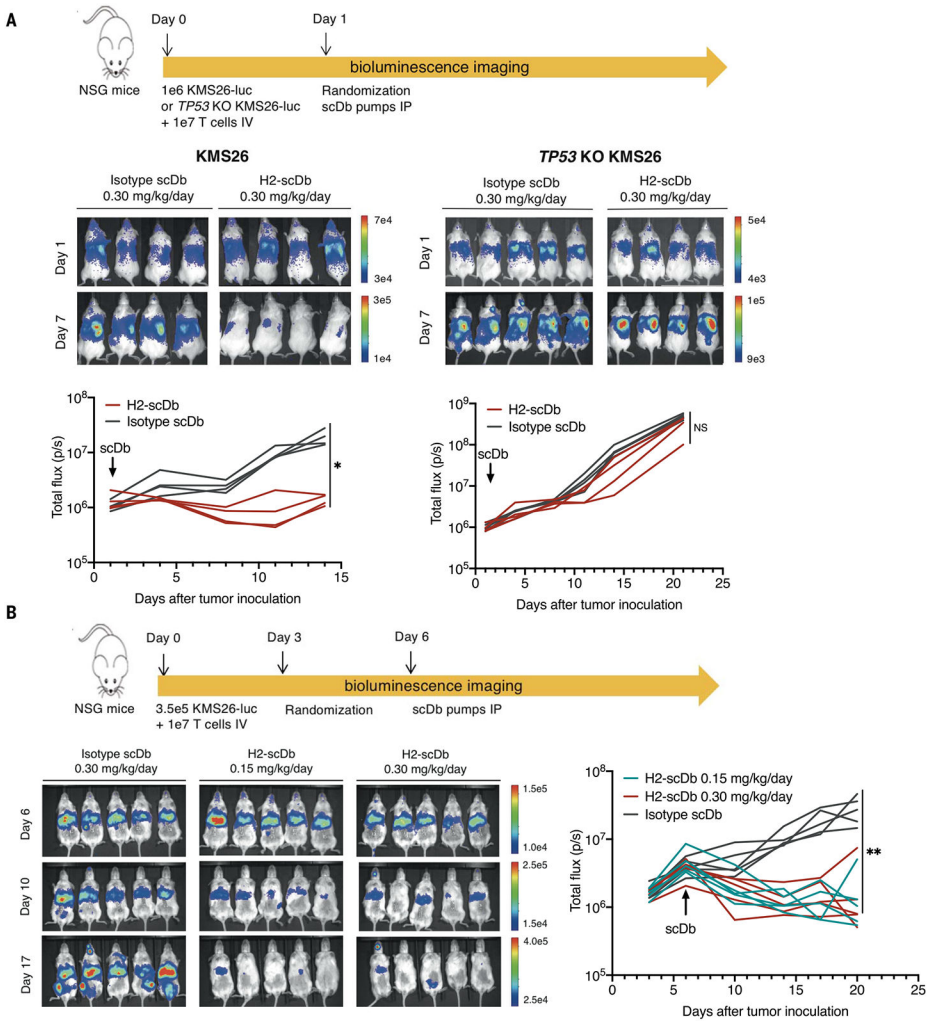

Fig. 6. In vivo antitumor efficacy of H2-scDb.

(**A**) In the early treatment model, NSG mice were engrafted through intravenous (IV) injection with 1×10^7 human T cells and either 1×10^6 parental KMS26 (left) or 1×10^6 *TP53* KO KMS26 (right) on day 0. On day 1, mice were randomized into treatment and control groups, and intraperitoneal (IP) infusion pumps were placed to administer H2-scDb or isotype control scDb at the specified infusion rate. *$P = 0.002$ and 0.012, NS $P = 0.084$ and 0.139 by means of two-tailed t test at the last time point with and without assuming equal variance, respectively. (**B**) In the established tumor model, NSG mice were engrafted with 1×10^7 human T cells and 3.5×10^5 parental KMS26 on day 0, followed by randomization on day 3 and IP placement of infusion pumps on day 6 to deliver H2-scDb or isotype scDb at the specified infusion rates. Tumor growth was monitored by means of bioluminescence imaging. $n = 4$ or 5 mice per group. Color bars denote the radiance (photons/s/cm^2/sr) scale at each time point. Plotted data indicate mean ± SD. **H2-scDb 0.15 mg/kg/day versus isotype scDb $P = 0.002$ and 0.009, H2-scDb 0.30 mg/kg/day versus Isotype scDb $P = 0.002$ and 0.009 by means of two-tailed t test at the last time point with and without assuming equal variance, respectively.